

On CSI-Free Multiantenna Schemes for Massive RF Wireless Energy Transfer

Onel L. A. López[✉], Member, IEEE, Samuel Montejo-Sánchez[✉], Member, IEEE,
 Richard D. Souza[✉], Senior Member, IEEE, Constantinos B. Papadias, Fellow, IEEE,
 and Hirley Alves[✉], Member, IEEE

Abstract—Radio-frequency wireless energy transfer (RF-WET) is emerging as a potential green enabler for massive Internet of Things (IoT). Herein, we analyze channel state information (CSI)-free multiantenna strategies for powering wirelessly a large set of single-antenna IoT devices. The CSI-free schemes are AA-SS (AA-IS), where all antennas transmit the same (independent) signal(s), and SA, where just one antenna transmits at a time such that all antennas are utilized during the coherence block. We characterize the distribution of the provided energy under correlated Rician fading for each scheme and find out that while AA-IS and SA cannot take advantage of the multiple antennas to improve the average provided energy, its dispersion can be significantly reduced. Meanwhile, AA-SS provides the greatest average energy, but also the greatest energy dispersion, and the gains depend critically on the mean phase shifts between the antenna elements. We find that consecutive antennas must be π -phase shifted for optimum average energy performance under AA-SS. Our numerical results evidence that correlation is beneficial under AA-SS, while a greater line of sight (LOS) and/or the number of antennas is not always beneficial under such a scheme. Meanwhile, both AA-IS and SA schemes benefit from small correlation, large LOS, and/or a large number of antennas. Finally, AA-SS (SA and AA-IS) is (are) preferable when devices are (are not) clustered in specific spatial directions. **AA-SS**

Index Terms—Channel state information (CSI) free, Internet of Things (IoT), massive radio-frequency wireless energy transfer (RF-WET), multiple antennas, phase shifts, Rician fading.

I. INTRODUCTION

INTERNET of Things (IoT), where every *thing* is practically transformed into an information source, represents a major

Manuscript received May 3, 2020; accepted June 13, 2020. Date of publication June 17, 2020; date of current version December 21, 2020. This work was supported in part by the Academy of Finland under Grant 307492, Grant 318927 (6Genesis Flagship), and Grant 319008 (EE-IoT); in part by the Finnish Foundation for Technology Promotion, FIREMAN under Grant 326301, in part by FONDECYT Regular Grant 1201893 in Chile, in part by the National Council for Scientific and Technological Development, and in part by the Project Print CAPES-UFSC “Automation 4.0” in Brazil. (*Corresponding author:* Onel L. A. López.)

Onel L. A. López and Hirley Alves are with the Centre for Wireless Communications, University of Oulu, 90014 Oulu, Finland (e-mail: onel.alcarazlopez@oulu.fi; hirley.alves@oulu.fi).

Samuel Montejo-Sánchez is with the Programa Institucional de Fomento a la I+D+i, Universidad Tecnológica Metropolitana, Santiago 8940577, Chile (e-mail: smontejo@utem.cl).

Richard D. Souza is with the Department of EEL, Federal University of Santa Catarina, Florianópolis 88040-900, Brazil (e-mail: richard.demo@ufsc.br).

Constantinos B. Papadias is with the Research, Technology and Innovation Network, American College of Greece, 15342 Athens, Greece (e-mail: cpapadias@acg.edu).

Digital Object Identifier 10.1109/JIOT.2020.3003114

technology trend that is revolutionizing the way we interact with our surrounding environment so that we can make the most of it. There are two general categories of IoT use cases [1]: 1) critical IoT, with stringent requirements on reliability, availability, and low latency, e.g., in remote healthcare, traffic safety and control, industrial applications and control, remote manufacturing, and surgery and 2) massive IoT, where sensors typically report to the cloud, and the requirement is for low-cost devices with low energy consumption and good coverage. In such massive deployments, these IoT nodes are not generally supposed to be transmitting continuously, but they do require to operate for long periods of time without batteries replacement, especially since many of them could be placed in hazardous environments, building structures, or the human body. One important enabler under consideration is wireless energy transfer (WET). Note that WET is a general concept that includes several power transfer technologies, such as those employing for instance ultrasound, inductive, capacitive, or resonant coupling [2]. In this work, we focus on radio frequency (RF)-based WET which allows the IoT nodes equipped with an energy harvesting (EH) circuitry to harvest energy from incoming RF signals [3]–[6]. Hereinafter, we refer to radio-frequency WET (RF-WET) just as WET.

WET holds vast potential for replacing batteries or increasing their lifespans. In fact, RF-EH devices can become self-sustaining with respect to the energy required for operation, thereby obtaining an unlimited operating lifespan while demanding negligible maintenance [7]. This is crucial for the future society since battery waste processing is already a critical problem. The most effective approach for reducing battery waste is to avoid using them, for which WET is an attractive clean solution. Note that with the continuous advances in circuitry technology aiming at reducing further the power consumption of low-cost devices,¹ e.g., advances on complementary metal-oxide semiconductor (CMOS) and micro-electro-mechanical systems (MEMSs)

¹Such current technological advances point to power consumption in the order of nW and μ W (or even less) in sleep and active modes, respectively. Nowadays, there is available a wide range of IoT devices that seem suitable for relying on an RF-EH module as the main power supply due to their extremely low-power consumption profiles. For instance, accelerometer ADXL362 ($\sim 40 \mu$ W in active) and light ISL29033 ($\sim 100 \mu$ W in active) [8]. In fact, the first wireless battery-free biosignal processing system on the chip was introduced by Zhang *et al.* [9] and it is able of monitoring various biosignals via electrocardiogram, electromyogram, and electroencephalogram. The total size of the chip is 8.25 mm² and consumes 19 μ W to measure the heart rate.

technologies [10], energy-efficient proportional to the absolute temperature (PTAT) circuit implementations [11], and printed sensors technology [12], an exponential growth on WET-enabled IoT applications is expected.

The IoT paradigm intrinsically includes wireless information transfer (WIT), thus WET appears naturally combined with WIT. In such case, two main architectures can be distinguished in the literature: 1) wireless powered communication network (WPCN), where WET occurs in the downlink in the first phase and WIT takes place in the second phase and 2) simultaneous wireless information and power transfer (SWIPT), where WET and WIT occur simultaneously. Readers can refer to [13] to review the recent progress on both architectures, while herein the discussions will focus merely on WPCN and pure WET setups. Note that in most practical applications, the WET duration would be significantly larger than WIT in order to harvest usable amounts of energy [6]. Actually, some use cases require operating under WET almost permanently while WIT happens sporadically, e.g., due to event-driven traffic. Therefore, enabling efficient WET is mandatory for realizing the IoT paradigm and constitutes the scope of this work.

A. Related Work

Recent works have specifically considered WET and WPCN setups in different contexts and scenarios. Key networking structures and performance-enhancing techniques to build an efficient WPCN are discussed in [14], where authors also point out challenging research directions. Departing from the simple harvest-then-transmit (HTT) scheme [15]–[17], several other protocols have been proposed over the past few years to boost the WPCN performance, such as the harvest-then-cooperate (HTC) system studied in [18]–[20] and the power control scheme relying on energy accumulation between transmission rounds discussed in [21]. The authors either analyzed the performance of the information transmission phase or optimized it by using power control or cooperative schemes. Some scheduling strategies that allow a direct optimization of the energy efficiency of the network are also proposed in [22] and [23]. Additionally, an energy cooperation scheme that enables energy cooperation in battery-free wireless networks with WET is presented in [24]. Meanwhile, the deployment of single-antenna power beacons (PBs) for powering the mobiles in an uplink cellular network is proposed in [25]. Therein, authors investigated the network performance under an outage constraint on data links using stochastic-geometry tools, while they corroborate the effectiveness of relying on directed WET instead of using isotropic antennas.

Yet, shifts in the system architecture and in the resource allocation strategies for optimizing the energy supply to massive IoT deployments are still required. In [6], we discuss several techniques that seem suitable for enabling WET as an efficient solution for powering the future IoT networks, which are as follows.

- 1) Energy beamforming (EB), which allows the energy signals at different antennas to be carefully weighed to achieve constructive superposition at intended receivers.

The larger the number of antennas installed at the PB, the sharper the energy beams can be generated in some particular spatial directions. The EB benefits for WPCNs have been investigated for instance in [26] in terms of average throughput performance, while Park *et al.* [27] proposed an EB scheme that maximizes the weighted sum of the harvested energy and the information rate in a multiple-input-single-output (MISO) system. However, the benefits of EB in practice depend on the available channel state information (CSI) at the transmitter, and although there have been some works proposing adequate channel acquisition methods, e.g., [28], [29], this still constitutes as a serious limitation. This is due to the harsh requirements in terms of energy and scheduling policies, which become even more critical as the number of EH devices increases.

- 2) Distributed antenna systems (DASs), which are capable of eliminating blind spots while homogenizing the energy provided to a given area and supporting ubiquitous energy accessibility. The placement optimization of single-antenna energy and information access points in WPCNs is investigated in [30], where authors focus on minimizing the network deployment cost subject to EH and communication performance constraints. On the other hand, Chen *et al.* [31] studied the probability density function (PDF), the cumulative distribution function (CDF), and the average of the energy harvested in DAS, while they determined appropriate strategies when operating under different channel conditions by using such information. Although works in this regard have avoided the use of multiple transmit antennas, we would like to highlight the fact that multiple separate PBs, each equipped with multiple transmit antennas, could alleviate the issue of CSI acquisition when forming efficient energy beams in multiple-users setups, since each PB may be responsible for the CSI acquisition procedure of a smaller set of EH devices.
- 3) CSI-limited/CSI-free schemes. Even without accounting for the considerable energy resources demanded by CSI acquisition, the performance of CSI-based systems decays quickly as the number of served devices increases. Therefore, in massive deployment scenarios, the broadcast nature of wireless transmissions should be intelligently exploited for powering simultaneously a massive number of IoT devices with minimum or non-CSI. For instance, Clerckx and Kim [32] proposed a method that relies on multiple dumb antennas transmitting phase-shifted signals to induce fast fluctuations on a slow-fading wireless channel and attain transmit diversity. Also, we recently analyzed in [33] several CSI-free multi-antenna schemes that a PB may utilize to efficiently power a large set of nearby EH devices, while we discussed their performance in Rician correlated fading channels. We found out that: a) the switching antenna (SA) strategy, where a single antenna transmits at a time with full power, provides the most predictable energy source, and it is particularly suitable for powering sensor nodes with highly sensitive EH hardware

operating under nonline of sight (NLOS) and b) transmitting simultaneously the same signal with equal power in all antennas [AA, but herein referred as all antennas transmitting the same signal (AA-SS)] is the most beneficial scheme when LOS increases and it is the only scheme that benefits from spatial correlation. Note that SA and AA-SS are, respectively, special cases of *unitary* and *uniform query* schemes proposed in the context of backscattering communications [34]. In fact, He *et al.* [34] and [35] showed that *unitary query* can provide considerable performance gains with respect to *uniform query*. However, such analyses do not consider the impact of the antenna array architecture on the LOS component of the channels, which herein we show to be significant. Finally, the performance analyses conducted in [33] were under the idealistic assumption of channels sharing the same mean phase.

B. Contributions and Organization of This Article

This article builds on CSI-free WET with multiple transmit antennas to power efficiently a large set of IoT devices. Different from our early work in [33], herein we do consider the mean phase shifts between antenna elements, which is a practical and unavoidable phenomenon. Based on such modeling, we arrive at conclusions that are similar in some cases but different in others to those in [33]. Specifically, the main contributions of this work can be listed as follows.

- 1) We analyze the CSI-free multiantenna strategies studied in [33], e.g., AA-SS and SA, in addition to the all antennas transmitting independent signals (AA-IS) scheme, but under **shifted mean phase channels**. We do not consider any other information related to devices, such as topological deployment and battery charge; although, such information could be crucial in some setups. Our derivations are specifically relevant for scenarios where it is difficult and/or not worth obtaining such information, e.g., when powering a massive number of low-power EH devices with null/limited feedback to the PB.
- 2) By considering the nonlinearity of the EH receiver, we demonstrated that those devices far from the PB and more likely to operate near their sensitivity level, benefit more from the SA scheme than from AA-IS. However, those closer to the PB and more likely to operate near saturation, benefit more from AA-IS.
- 3) We attain the distribution and some main statistics of the RF energy at the EH receiver in correlated Rician fading channels under each WET scheme. Note that the Rician fading assumption is general enough to include a class of channels, ranging from Rayleigh fading channel without LOS to a fully deterministic LOS channel, by varying the Rician factor κ .
- 4) While AA-IS and SA cannot take advantage of the multiple antennas to improve the average statistics of the incident RF power, the energy dispersion can be significantly reduced, thus reducing the chances of energy outage. Meanwhile, the gains attained by AA-SS in terms of average RF energy delivery depend critically

on the mean phase shifts between the antenna elements. In that regard, we show the considerable performance gaps between the idealistic AA-SS analyzed in [33] and this scheme when considering channels with different mean phases. Even under such performance degradation, AA-SS still provides the greatest average harvested energy when compared to AA-IS and SA but its associated energy outage probability is generally the worst.

- 5) We attained the optimum preventive phase shifting for maximizing the average energy delivery or minimizing its dispersion for each of the schemes. We found that when transmitting the same signal simultaneously over all the antennas (AA-SS or equivalently AA in [33]), consecutive antennas must be π -phase shifted for optimum performance. Meanwhile, under different schemes there is **no need** of carrying out any preventive phase shifting. Note that all the analyzed CSI-free schemes, in their nonoptimized form, say without proactive phase shifting, are special cases of the *uniform* (AA-SS) and *unitary query* schemes (AA-IS and SA) in the context of backscattering communications [34], however, they differ conceptually (and also in terms of performance in the case of AA-SS) when phase shifts are applied to the signals.
- 6) Our numerical results corroborate that correlation is beneficial under AA-SS, especially under poor LOS where channels are more random. A very counter-intuitive result is that a greater LOS and/or the number of antennas is not always beneficial when transmitting the same signal simultaneously through all antennas. Meanwhile, since correlation (LOS and the number of antennas) is well known to decrease (increase) the diversity, AA-IS and SA schemes are affected by (benefited from) an increasing correlation (LOS factor and the number of antennas).
- 7) While most of the analytical derivations are obtained under the assumption that devices' positioning information is not available and/or they are uniformly distributed in the area, we show how the analyzed schemes can still be efficiently utilized to fairly power massive deployments when such assumptions do not hold. For instance, AA-SS (SA and AA-IS) is (are) preferable when devices are (are not) clustered in specific spatial directions.

The remainder of this article is organized as follows. Section II presents the system model, while Section III presents and discusses the CSI-free WET strategies. Their performance under Rician fading is investigated in Sections IV and V, while Section VI presents numerical results. Finally, Section VII concludes the article.

Notation: Boldface lowercase letters denote column vectors, while boldface uppercase letters denote matrices. For instance, $\mathbf{x} = \{x_i\}$, where x_i is the i th element of vector \mathbf{x} ; while $\mathbf{X} = \{X_{i,j}\}$, where $X_{i,j}$ is the i th row j th column element of matrix \mathbf{X} . By \mathbf{I} we denote the identity matrix, and by $\mathbf{1}$ we denote a vector of ones. Superscripts $(\cdot)^T$ and $(\cdot)^H$ denote the transpose and conjugate transpose operations, respectively, while $\det(\cdot)$ is the determinant, and by $\text{diag}(x_1, x_2, \dots, x_n)$ we

denote the diagonal matrix with elements x_1, x_2, \dots, x_n . \mathcal{C} and \mathcal{R} are the set of complex and real numbers, respectively; while $\mathbf{i} = \sqrt{-1}$ is the imaginary unit. Additionally, $|\cdot|$ and $\text{mod}(a, b)$ are the absolute and modulo operations, respectively, while $\|\mathbf{x}\|$ denotes the euclidean norm of \mathbf{x} . $\mathbb{E}[\cdot]$ and $\text{var}[\cdot]$ denote expectation and variance, respectively, while $\Pr[A]$ is the probability of event A . $\mathbf{v} \sim \mathcal{N}(\boldsymbol{\mu}, \mathbf{R})$ and $\mathbf{w} \sim \mathcal{CN}(\boldsymbol{\mu}, \mathbf{R})$ are a Gaussian real random vector and a circularly-symmetric Gaussian complex random vector, respectively, with mean vector $\boldsymbol{\mu}$ and covariance matrix \mathbf{R} . Additionally, $p_Y(y)$ denotes the PDF of random variable (RV) Y , while $Z \sim \chi^2(m, n)$ is a noncentral chi-squared RV with m degrees of freedom and parameter n . Then, according to [36, eq. (2-1-125)] the first two central moments are given by $\mathbb{E}[Z] = m + n$ and $\text{var}[Z] = 2(m + 2n)$. Finally, $J_0(\cdot)$ denotes the Bessel function of the first kind and order 0 [37, Sec. 10.2].

II. SYSTEM MODEL MISO

Consider the scenario in which a PB equipped with M antennas powers wirelessly a large set $\{S_i\}$ of single-antenna sensor nodes located nearby. Since this work deals only with CSI-free WET schemes, and for such scenarios the characterization of one sensor is representative of the overall performance, we focus our attention on the case of a generic node S . The fading channel coefficient between the j th PB's antenna and S is denoted as $h_j \in \mathcal{C}$, $j \in \{1, \dots, M\}$, while $\mathbf{h} \in \mathcal{C}^{M \times 1}$ is a vector with all the antennas' channel coefficients.

A. Channel Model

Quasistatic channels are assumed, where the fading process is considered to be constant over the transmission of a block and independent and identically distributed (i.i.d.) from block to block. Without loss of generality, we set the duration of a block to 1 so the terms energy and power can be indistinctly used. Specifically, we consider channels undergoing Rician fading, which is a very general assumption that allows modeling a wide variety of channels by tuning the Rician factor $\kappa \geq 0$ [36, Ch. 2], e.g., when $\kappa = 0$, the channel envelope is Rayleigh distributed, while when $\kappa \rightarrow \infty$ there is a fully deterministic LOS channel. Therefore

$$\mathbf{h} = \sqrt{\frac{\kappa}{1+\kappa}} e^{i\varphi_0} \mathbf{h}_{\text{los}} + \sqrt{\frac{1}{1+\kappa}} \mathbf{h}_{\text{nlos}} \quad (1)$$

is the normalized channel vector [38, Ch. 5], where $\mathbf{h}_{\text{los}} = [1, e^{i\Phi_1}, \dots, e^{i\Phi_{M-1}}]^T$ is the deterministic LOS propagation component such that Φ_t , $t \in \{1, \dots, M-1\}$ is the mean phase shift of the $(t+1)$ th array element with respect to the first antenna. Additionally, φ_0 accounts for an initial phase shift, while $\mathbf{h}_{\text{nlos}} \sim \mathcal{CN}(\mathbf{0}, \mathbf{R})$ represents the scattering (Rayleigh) component. We assume a real covariance matrix $\mathbf{R} \in \mathcal{R}^{M \times M}$ for gaining in analytical tractability, which means that real and imaginary parts of \mathbf{h}_{nlos} are i.i.d. and also with covariance \mathbf{R} [39]. Assume half-wavelength equally spaced antenna elements, e.g., as in a uniform linear array (ULA), yielding

$$\Phi_t = -\pi t \sin \phi \quad (2)$$

where $\phi \in [0, 2\pi]$ is the azimuth angle relative to the bore-sight of the transmitting antenna array. Such angle depends on

both transmit and receive local conditions, e.g., antenna orientation and node's location, and consequently it is different for each sensor S . Additionally, let us denote by β the average RF power available at S if the PB transmits with full power over a single antenna. Under such a single-antenna setup, the available RF energy at the input of the EH circuitry is given by $\beta|h_{i^*}|^2$, where i^* is the index of the active antenna. Note that β includes the effect of both path loss and transmit power.

B. Preventive Adjustment of Mean Phases

As mentioned earlier, ϕ and consequently, Φ are different for each sensor, which prevents us from making any preventive phase adjustment based on specific ϕ . However, maybe we could still use the topological information embedded in (2), which tell us that Φ_t increases with t for a given ϕ , to improve the statistics of the harvested energy. To explore this, let us consider that the PB applies a preventive adjustment of the signal phase at the $(t+1)$ th array element given by $\psi_t \in [0, 2\pi]$, while without loss of generality we set $\psi_0 = 0$. Then, the equivalent normalized channel vector seen at certain sensor S becomes $\mathbf{h}^* = \Psi \mathbf{h}$, where

$$\Psi = \text{diag}\left(1, e^{i\psi_1}, \dots, e^{i\psi_{M-1}}\right). \quad (3)$$

Now, departing from (1) we have that

$$\begin{aligned} \mathbf{h}^* &= \sqrt{\frac{\kappa}{1+\kappa}} e^{i\varphi_0} \Psi \mathbf{h}_{\text{los}} + \sqrt{\frac{1}{1+\kappa}} \Psi \mathbf{h}_{\text{nlos}} \\ &\sim \sqrt{\frac{\kappa}{1+\kappa}} e^{i\varphi_0} \underbrace{\left[1, e^{i(\Phi_1+\psi_1)}, \dots, e^{i(\Phi_{M-1}+\psi_{M-1})}\right]^T}_{\Psi \mathbf{h}_{\text{los}}} \\ &\quad + \sqrt{\frac{1}{1+\kappa}} \mathcal{CN}(\mathbf{0}, \mathbf{R}) \underbrace{\mathbf{h}_{\text{nlos}}}_{\Psi \mathbf{h}_{\text{nlos}}} \end{aligned} \quad (4)$$

where last line comes from simple algebraic operations and using the fact that $\Psi \mathbf{h}_{\text{nlos}} \sim \mathcal{CN}(\mathbf{0}, \Psi \mathbf{R} \Psi^H) \sim \mathcal{CN}(\mathbf{0}, \mathbf{R})$ since Ψ is diagonal with unit absolute values' entries. Without loss of generality, by conveniently setting $\varphi_0 = \pi/4$ [40] so $e^{i\varphi_0} = (1+i)/\sqrt{2}$ imposes the effect of LOS (constant) component on real and imaginary parts of the scattering (Rayleigh) component \mathbf{h}_{nlos} , we rewrite (4) as $\mathbf{h}^* = \mathbf{h}_x + i\mathbf{h}_y$, where \mathbf{h}_x and \mathbf{h}_y are independently distributed as

$$\mathbf{h}_{x,y} \sim \sqrt{\frac{1}{2(\kappa+1)}} \mathcal{N}(\sqrt{\kappa} \omega_{x,y}, \mathbf{R}) \quad (5)$$

where $\omega_{x,y} = [1, \cos(\Phi_1 + \psi_1) \mp \sin(\Phi_1 + \psi_1), \dots, \cos(\Phi_{M-1} + \psi_{M-1}) \mp \sin(\Phi_{M-1} + \psi_{M-1})]^T$.

C. EH Transfer Function

Finally, and after going through the channel, the RF energy is harvested at the receiver end. The EH circuitry is characterized by a nondecreasing function $g : \mathcal{R}^+ \mapsto \mathcal{R}^+$ modeling the relation between the incident and harvested RF power² at S . With such a function in place, the power transfer efficiency (PTE) is given by $g(x)/x$. In most of the works, g is assumed to be linear for analytical tractability, e.g., [15]–[20], [22],

²In practice, g also depends on the modulation and incoming waveform [32], [41].

$$\text{又: } \frac{\Delta t}{f} = \frac{2\pi}{\lambda} \Rightarrow \lambda = 2\pi f \Delta t = \pi \frac{s \sin \phi}{f} = \pi s \sin \phi.$$

and [24]–[30], which implies that $g(x) = \eta x$ where η is a PTE constant, thus independent of the input power. However, in practice, the PTE actually depends on the input power and consequently, the relationship between the input power and the output power is nonlinear [13], [31], [33], [42]. In this work, we consider the following EH transfer function [42]:

$$g(x) = g_{\max} \left(\frac{1 + e^{ab}}{1 + e^{-a(x-b)}} - 1 \right) e^{-ab} \quad (6)$$

which is known to describe accurately the nonlinearity of EH circuits by properly fitting parameters $a, b \in \mathbb{R}^+$, while g_{\max} is the harvested power at saturation.

III. CSI-FREE MULTIANTENNA WET STRATEGIES

Herein, we overview CSI-free multiple-antenna WET strategies for efficient wireless powering, while discussing some related practicalities.

A. All Antennas Transmitting the Same Signal

Under this scheme, the PB transmits the same signal s simultaneously with all antennas and with equal power at each. Such scheme (in its nonoptimized form) is referred to as *uniform query* in the context of backscattering communications [34] and as AA in [33]. Herein, we refer to it as AA-SS to explicitly highlight its difference with respect to the AA-IS scheme (see next section). Under this scheme, the RF signal at the receiver side and ignoring the noise, whose energy is negligible for harvesting,³ are given by $\sum_{j=1}^M \sqrt{(\beta/M)} h_j^* s$, where s is normalized such that $\mathbb{E}[s^H s] = 1$. Then, the energy harvested by S is given by

$$\xi_{\text{aa-ss}} = g(\xi_{\text{aa-ss}}^{\text{rf}}) \quad (7)$$

where

$$\begin{aligned} \xi_{\text{aa-ss}}^{\text{rf}} &= \mathbb{E}_s \left[\left(\sum_{j=1}^M \sqrt{\frac{\beta}{M}} h_j^* s \right)^H \left(\sum_{j=1}^M \sqrt{\frac{\beta}{M}} h_j^* s \right) \right] \\ &= \mathbb{E}_s \left[\sum_{j=1}^M \sqrt{\frac{\beta}{M}} h_j^* \left| s \right|^2 s^H s \right] \quad \text{功率/能量 (平均时间)} \\ &= \left| \sum_{j=1}^M \sqrt{\frac{\beta}{M}} h_j^* \right|^2 \mathbb{E}[s^H s] = \frac{\beta}{M} |\mathbf{h}^*|^2 \quad \text{功率/能量 (单个块)} \end{aligned}$$

is the available RF energy. Note that the terms energy and power can be used indistinctly since the block duration is normalized and the PB does not change its strategy over time.

B. All Antennas Transmitting Independent Signals

Instead of transmitting the same signal over all antennas, the PB may transmit signals s_j independently generated across the antennas. This is for alleviating the issue of destructive signal

³In WET setups, the performance depends on the available energy at the input of the energy harvester, which requires to be significant, at least in the order of sub-μW in the case of high sensitive EH hardware. Therefore, the noise impact is practically null, as widely recognized in the literature, e.g., [4], [13], [15]–[21], [26]–[30], [33], and [42].

combination at s , and constitutes a special case of the so-called *unitary query* in the context of backscattering communications [34]. We refer to this scheme as AA-IS, for which the RF signal at the receiver side and ignoring the noise, whose energy is negligible for harvesting, are given by $\sum_{j=1}^M \sqrt{(\beta/M)} h_j^* s_j$, where each s_j is normalized such that $\mathbb{E}[s_j^H s_j] = 1 \forall j$. Then, the harvested energy is given by

$$\xi_{\text{aa-is}} = g(\xi_{\text{aa-is}}^{\text{rf}}), \text{ where} \quad (9)$$

$$\begin{aligned} \xi_{\text{aa-is}}^{\text{rf}} &= \mathbb{E}_s \left[\left(\sum_{j=1}^M \sqrt{\frac{\beta}{M}} h_j^* s_j \right)^H \left(\sum_{j=1}^M \sqrt{\frac{\beta}{M}} h_j^* s_j \right) \right] \quad \text{因为 射频 功率? 不一样的才能将 S} \\ &= \mathbb{E}_s \left[\sum_{j=1}^M \left| \sqrt{\frac{\beta}{M}} h_j^* \right|^2 s_j^H s_j \right] = \frac{\beta}{M} \sum_{j=1}^M \left| h_j^* \right|^2 \mathbb{E}[s_j^H s_j] \quad \text{拿掉} \\ &= \frac{\beta}{M} \|\mathbf{h}^*\|^2. \end{aligned} \quad (10)$$

For both, AA-SS and AA-IS, the signal power over each antenna is $1/M$ of the total available transmit power. Additionally, note that M RF chains are required since all the antennas are simultaneously active. This is different from the CSI-free scheme discussed next.

C. Switching Antennas

Instead of transmitting with all antennas at once, the PB may transmit the (same or different) signal s with full power by one antenna at a time such that all antennas are used during a block. This is the SA scheme analyzed in [33], while it also constitutes a special case of the *unitary query* method in backscattering communications [34]. In this case, just one RF chain is required, hence reducing circuit power consumption, hardware complexity, and consequently the economic cost.

Assuming equal-time allocation for each antenna, the system is equivalent to that in which each subblock duration is $1/M$ of the total block duration, and the total harvested energy accounts for the sum of M subblocks. The RF signal at the receiver side during the j th subblock, and ignoring the noise, whose energy is negligible for harvesting, is given by $\sqrt{\beta} h_j^* s$, where s is normalized such that $\mathbb{E}[s^H s] = 1$, then

$$\xi_{\text{sa}} = \frac{1}{M} \sum_{j=1}^M g(\xi_{\text{sa},j}^{\text{rf}}) \quad (11)$$

where

$$\begin{aligned} \xi_{\text{sa},j}^{\text{rf}} &= \mathbb{E}_s \left[\left(\sqrt{\beta} h_j^* s \right)^H \left(\sqrt{\beta} h_j^* s \right) \right] = \mathbb{E}_s \left[\left| \sqrt{\beta} h_j^* \right|^2 s^H s \right] \\ &= \beta |h_j^*|^2 \mathbb{E}[s^H s] = \beta |h_j^*|^2 \end{aligned} \quad (12)$$

is the incident RF power during the j th subblock.

Note that for the simple, but commonly adopted in the literature, the linear EH model, both (9) and (11) matches. However, in practice $g(x)$ is nonlinear, and consequently (9) may differ significantly from (11). We depart from (6) to write the second derivative of $g(x)$ as

$$\frac{d^2}{dx^2} g(x) = \frac{a^2 e^{ax} (1 + e^{ab}) (e^{ab} - e^{ax}) g_{\max}}{(e^{ab} + e^{ax})^3} \quad (13)$$

which allows us to conclude that g is convex (concave) for $x \leq b$ ($x \geq b$). Then, for certain channel vector realization \mathbf{h} and using Jensen's inequality, we have that

$$g\left(\frac{\beta}{M} \sum_{j=1}^M |h_j|^2\right) \begin{cases} \leq \frac{1}{M} \sum_{j=1}^M g(\beta|h_j|^2), & \text{if } |h_j|^2 \leq \frac{b}{\beta} \forall j \\ \geq \frac{1}{M} \sum_{j=1}^M g(\beta|h_j|^2), & \text{if } |h_j|^2 \geq \frac{b}{\beta} \forall j \end{cases}$$

$$\xi_{\text{aa-is}} = \begin{cases} \leq \xi_{\text{sa}}, & \text{if } \max |h_j|^2 \leq \frac{b}{\beta} \\ \geq \xi_{\text{sa}}, & \text{if } \min |h_j|^2 \geq \frac{b}{\beta}. \end{cases} \quad (14)$$

Remark 1: The above result implies that devices far from the PB and more likely to operate near their sensitivity level, benefit more from the SA scheme than from AA-IS. However, those closer to the PB and more likely to operate near saturation, benefit more from AA-IS.

In the following, we analyze the statistics of the RF energy available at S for harvesting under the AA-SS and AA-IS schemes. For such schemes, the harvested energy comes from mapping the RF energy through the EH transfer function g , as shown in (7) and (9). For SA, the mapping is much more convoluted, especially because the available RF energy varies (although possibly correlational) within the same coherence block as illustrated in (11). However, our analysis in the previous paragraphs suggests that the statistics of $\xi_{\text{aa-is}}$ and ξ_{sa} may be approximated, which is an issue we discuss numerically in detail in Section VI.

IV. RF AVAILABLE ENERGY UNDER AA-SS

Next, we characterize the distribution of the RF power at S under the AA-SS scheme.

Theorem 1: Conditioned on the mean phase shifts of the powering signals, the distribution of the RF power at the input of the energy harvester under the AA-SS operation is given by

$$\xi_{\text{aa-ss}}^{\text{rf}} \sim \frac{\beta R_{\Sigma}}{2(\kappa+1)M} \chi^2\left(2, \frac{2\kappa f(\psi, \phi)}{R_{\Sigma}}\right) \quad (15)$$

where $R_{\Sigma} = \mathbf{1}^T \mathbf{R} \mathbf{1}$

$$f(\psi, \phi) = v_1(\psi, \phi)^2 + v_2(\psi, \phi)^2 \quad (16)$$

$$v_1(\psi, \phi) = 1 + \sum_{t=1}^{M-1} \cos(\psi_t + \Phi_t) \quad (17)$$

and Φ_t is given in (2) as a function of ϕ .

Proof: See Appendix A. ■

Note that (15) matches [33, eq. (25)] just in the specific case of unshifted mean phases, e.g., $\psi + \Phi = \mathbf{0}$. In such case, $f(\psi, \phi)$ becomes M^2 .

A. On the Impact of Different Phase Means

The impact of different phase means on the system performance is strictly determined by $f(\psi, \phi)$ in (15), and can be better understood by checking the main statistics, e.g., mean and variance, of the incident RF power, which can be

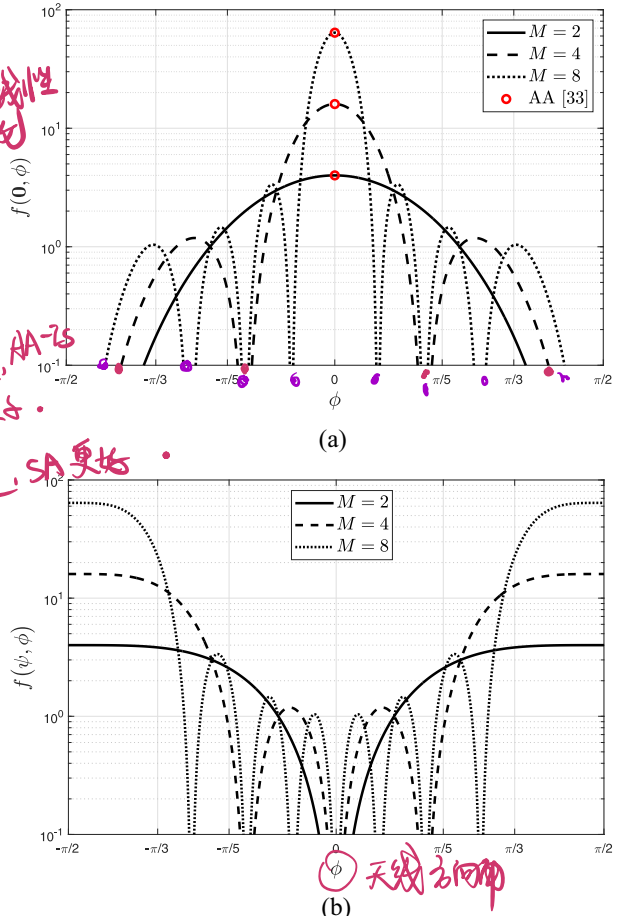


Fig. 1. (a) $f(\mathbf{0}, \phi)$ vs ϕ (top). (b) $f(\psi, \phi)$ vs ϕ for ψ according to (23) (bottom). We set $M \in \{2, 4, 8\}$.

$$\text{Koopman } \{E[X^2] = m+n\}$$

easily obtained from (15) by using $D[X^2] = 2(m+n)$

$$\mathbb{E}\left[\xi_{\text{aa-ss}}^{\text{rf}}\right] = \frac{\beta R_{\Sigma}}{2(\kappa+1)M} \left(2 + \frac{2\kappa}{R_{\Sigma}} f(\psi, \phi)\right)$$

$$= \frac{\beta}{M(\kappa+1)} (R_{\Sigma} + \kappa f(\psi, \phi)) \quad (18)$$

$$\text{var}\left[\xi_{\text{aa-ss}}^{\text{rf}}\right] = \frac{\beta^2 R_{\Sigma}^2}{4(\kappa+1)^2 M^2} \left(4 + \frac{8\kappa}{R_{\Sigma}} f(\psi, \phi)\right)$$

$$= \frac{\beta^2 R_{\Sigma}}{(\kappa+1)^2 M^2} (R_{\Sigma} + 2\kappa f(\psi, \phi)). \quad (19)$$

AA-SS 值

Therefore, both mean and variances increases with $f(\psi, \phi)$. Meanwhile, it is easy to check that $f(\psi, \phi)$ is maximized for $\psi + \Phi = \mathbf{0}$, for which $f(\psi, \phi) = M^2$, thus the entire analysis carried out in [33] on this AA-SS scheme provides upper bounds for both the mean and variance of the harvested energy. However, different phase means cause, in practice, a degradation on the diversity order of ξ^{rf} . Let us assume no preventive adjustment of mean phases is carried out, e.g., $\psi = \mathbf{0}$, to illustrate in Fig. 1(a) the impact of such different channel phase means. Specifically, we show $f(\mathbf{0}, \phi)$ for different values of M . Note that the performance diverges fast from the one claimed in [33] as ϕ moves away from 0.

由脚注的，随 $M \uparrow$, $f(\psi, \phi)$ 取 10^{-1} (表示 minima 的可能性更多) 从 0 零限

Remark 2: The number of minima of $f(\psi, \phi)$ matches M , thus as M increases, the chances of operating close to a minimum increase as well, which deteriorates significantly the system performance in terms of average incident RF power.

B. Preventive Adjustment of Mean Phases

Herein, we discuss how to set the vector ψ for optimizing the system performance. For clarity, and using (17) followed by some algebraic transformations, we rewrite (16) as follows:

$$\begin{aligned} f(\psi, \phi) &= \left(1 + \sum_{t=1}^{M-1} \cos(\Phi_t + \psi_t)\right)^2 + \left(\sum_{t=1}^{M-1} \sin(\Phi_t + \psi_t)\right)^2 \\ &= M + 2 \sum_{t=1}^{M-1} \cos(\Phi_t + \psi_t) \\ &\quad + 2 \sum_{t=1}^{M-2} \sum_{l=t+1}^{M-1} \cos(\Phi_t + \psi_t - \Phi_l - \psi_l). \end{aligned} \quad (20)$$

Assume ϕ uniformly distributed in $[0, 2\pi]$,⁴ e.g., $p_\phi(\phi) = (1/2\pi)$, then the problem translates to optimize over $f(\psi) = (1/2\pi) \int_0^{2\pi} f(\psi, \phi) d\phi$. Substituting (2) into (20) and integrating over ϕ we attain

使用 Bessel 将 Φ 和 ψ 转化为 ψ

$$\begin{aligned} f(\psi) &= M + 2 \sum_{t=1}^{M-1} J_0(t\pi) \cos \psi_t \\ &\quad + 2 \sum_{t=1}^{M-2} \sum_{l=t+1}^{M-1} J_0((t-l)\pi) \cos(\psi_t - \psi_l) \end{aligned} \quad (21)$$

which comes from using the integral representation of $J_0(\cdot)$ [37, eq. (10.9.1)]. Obviously, (18) and (19) still hold but using $f(\psi)$ instead of $f(\psi, \phi)$.

1) Average Energy Maximization: Solving the problem of maximizing, the average incident RF power is equivalent to solve $\arg \max_{\psi} f(\psi)$. Now, since $|\cos \alpha| \leq 1$ we have that

$$f(\psi) \leq M + 2 \sum_{t=1}^{M-1} |J_0(t\pi)| + 2 \sum_{t=1}^{M-2} \sum_{l=t+1}^{M-1} |J_0((t-l)\pi)|. \quad (22)$$

Using the fact that $J_0(t\pi)$ is positive (negative) if t is even (odd), we can easily observe that the upper bound in (22) can be attained by setting $\psi_t = 0 (\pi)$ for t even (odd) in (21), e.g.,

$$\psi_t = \mod(t, 2)\pi, \quad t \in \{0, 1, \dots, M-1\}. \quad (23)$$

Remark 3: The above results mean that consecutive antennas must be π -phase shifted for optimum average energy performance under the AA-SS scheme.

Despite optimum $f(\psi)$ as in (22) cannot be simplified, an accurate approximation is

$$f(\psi) \approx 0.85 \times M^{1.5} \quad (24)$$

which comes from standard curve fitting.

⁴This fits scenarios where θ corresponding to each sensor is unknown, or alternatively, scenarios where there is a very large number of sensors homogeneously distributed in space such that $p_\phi(\phi) \approx (1/2\pi)$. Although our analysis here holds specifically for such uniform angle distribution, our procedures and ideas can be extended to other scenarios.

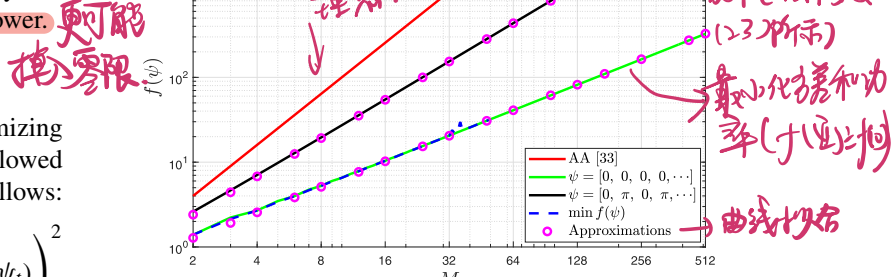


Fig. 2. $f(\psi)$ versus M .

In Fig. 1(b), we show the impact of the above preventive phase shifting on $f(\psi, \phi)$ for different angles ϕ . By comparing Fig. 1(a) (no preventive phase shifting) and (b) [preventive phase shifting given in (23)], note that: 1) the number of minima keeps the same; 2) the best performance occurs now for $\phi = \pm\pi/2$, while the worst situation happens when $\phi = 0$; and 3) there are considerable improvements in terms of area under the curves, which are expected to conduce to considerable improvements when averaging over ϕ .

2) Energy Dispersion Minimization: As a metric of dispersion, we consider the variance. Therefore, herein, we aim to solve $\arg \min_{\psi} f(\psi)$; although note that this in turn minimizes the average available RF energy as well.⁵

Different from the maximization problem, the problem of minimizing $f(\psi)$ is not such easy to handle. We resorted to MATLAB numerical solvers and realized that optimal solutions diverge significantly for different values of M . However, we found that $f(\mathbf{0})$ approximates extraordinarily to the optimum function value. Therefore, $\psi = \mathbf{0}$ minimizes the variance of the incident RF power, and no preventive phase shifting is required in this case. This means that

$$\begin{aligned} f(\psi) &\gtrsim f(\mathbf{0}) \\ &= M + 2 \sum_{t=1}^{M-1} J_0(t\pi) + 2 \sum_{t=1}^{M-2} \sum_{l=t+1}^{M-1} J_0((t-l)\pi) \\ &\stackrel{(a)}{\approx} 0.64 \times M \end{aligned} \quad (25)$$

where (a) comes from standard curve fitting.

Remark 4: Results in (24) and (25) evidence that both $\max f(\psi)$ and $\min f(\psi)$ share a polynomial dependence on M . In the case of $\min f(\psi)$, such relation is linear while $\max f(\psi)$ is roughly \sqrt{M} times greater than $\min f(\psi)$.

3) Validation: In Fig. 2, we show $f(\psi)$ as a function of M for: 1) the phase shifting in (23), which maximizes the average incident RF power; 2) $\psi = \mathbf{0}$, e.g., no preventive phase shifting, which minimizes both the variance and average statistics; and 3) the scenario discussed in [33], which is constrained to $\psi = \Phi = \mathbf{0}$. We utilized MATLAB numerical optimization

⁵It is easily verifiable that the phase shifting that satisfies $\arg \min_{\psi} f(\psi)$, minimizes the coefficient of variation parameter, which is given by $[(\sqrt{\text{var}[\xi]}) / (\mathbb{E}[\xi])]$, and constitutes probably a more suitable dispersion metric.

solvers for minimizing $f(\psi)$, but such approach was efficient just for $M \leq 32$. For a greater M , MATLAB solvers do not always converge and are extremely time consuming. Meanwhile, note that $\psi = \mathbf{0}$ indeed approaches extremely to $\arg \min_{\psi} f(\psi)$. The approximations in (24) and (25) are accurate.

4) On the Optimization Gains: By using (18), (24), and (25), the dB gain in average incident RF energy with respect to the nonpreventive shifting scheme, which in turn minimizes the energy dispersion according to our discussion in Section IV-B2, can be obtained as follows:

$$\begin{aligned}\delta_E &\approx 10 \log_{10} \left(\frac{\beta(R_\Sigma + 0.85\kappa M^{1.5})}{M(\kappa + 1)} \right) / \left(\frac{\beta(R_\Sigma + 0.64\kappa M)}{M(\kappa + 1)} \right) \\ &= 10 \log_{10} \left(\frac{R_\Sigma + 0.85\kappa M^{1.5}}{R_\Sigma + 0.64\kappa M} \right) \\ &\geq 10 \log_{10} \left(\frac{M + 0.85\kappa \sqrt{M}}{M + 0.64\kappa} \right)\end{aligned}\quad (26)$$

where last line comes from the fact that the argument of the logarithm is a decreasing function of R_Σ since $0.85\kappa M^{1.5} > 0.64\kappa M$ for $M \geq 2$, and $R_\Sigma \leq M^2$.

Now, we evaluate the costs in terms of the variance increase of such average energy maximization shifting. By using (19), (24), and (25) we have that

$$\begin{aligned}\delta_{\text{var}} &\approx 10 \log_{10} \left(\frac{R_\Sigma + 2 \times 0.85\kappa M^{1.5}}{R_\Sigma + 2 \times 0.64\kappa M} \right) \\ &\stackrel{(a)}{\leq} 10 \log_{10} \left(\frac{2 \times 0.85\kappa \sqrt{M}}{2 \times 0.64\kappa} \right) \\ &= 5 \log_{10} M + 1.23\end{aligned}\quad (27)$$

where (a) comes from using the lower bound of R_Σ , e.g., $R_\Sigma \geq 0$. The above results imply for instance that the gain in the average incident RF energy is above 3.47 dB when $\kappa = 10$ and $M = 8$, while the variance can increase to 5.75 dB maximum as well.

V. RF AVAILABLE ENERGY UNDER AA-IS

Next, we characterize the distribution of the RF power at the receiver end under the AA-IS scheme.

Theorem 2: Conditioned on the mean phase shifts of the powering signals, the approximated distribution of the RF power available as input to the energy harvester under the AA-IS is

$$\begin{aligned}\xi_{\text{aa-is}}^{\text{rf}} &\sim \frac{\beta}{2M^2(\kappa + 1)} \left(R_\Sigma \chi^2 \left(2, \frac{2\kappa f(\psi, \phi)}{R_\Sigma} \right) \right. \\ &\quad \left. + \frac{M^2 - R_\Sigma}{M - 1} \chi^2 \left(2(M - 1), \frac{2M(M - 1)\kappa \tilde{v}(\psi, \phi)}{M^2 - R_\Sigma} \right) \right)\end{aligned}\quad (28)$$

where

$$\begin{aligned}\tilde{v}(\psi, \phi) &= M - 1 + 2 \sum_{j=1}^{M-1} \frac{1}{j(j+1)}$$

$$\begin{aligned}&\times \left(\sum_{t=M-j+1}^{M-1} \cos(\psi_t + \Phi_t) + \sum_{t=M-j+1}^{M-1} \sum_{l=t+1}^{M-1} \right. \\ &\quad \times \cos(\psi_t + \Phi_t - \psi_l - \Phi_l) - j \cos(\psi_{M-j} + \Phi_{M-j}) \\ &\quad \left. - j \sum_{t=M-j+1}^{M-1} \cos(\psi_{M-j} + \Phi_{M-j} - \psi_t - \Phi_t) \right).\end{aligned}\quad (29)$$

Proof: See Appendix B. ■

For $\psi + \Phi = \mathbf{0}$, (28) matches [33, eq. (39)].⁶ However, when mean phase shifts between antenna elements increase, both expressions diverge.

A. On the Impact of Different Mean Phases

It is not completely clear from (28) whether phase shifts are advantageous or not under this scheme. Let us start by checking the average statistics of $\xi_{\text{aa-is}}^{\text{rf}}$ as follows:

$$\begin{aligned}\mathbb{E}[\xi_{\text{aa-is}}^{\text{rf}}] &\approx \frac{\beta}{2M^2(\kappa + 1)} \left(\frac{M^2 - R_\Sigma}{M - 1} \left(2(M - 1) + \frac{2M(M - 1)\kappa \tilde{v}(\psi, \phi)}{M^2 - R_\Sigma} \right) \right. \\ &\quad \left. + R_\Sigma \left(2 + \frac{2\kappa f(\psi, \phi)}{R_\Sigma} \right) \right) \\ &= \frac{\beta}{M^2(\kappa + 1)} (M^2 - R_\Sigma + M\kappa \tilde{v}(\psi, \phi) + R_\Sigma + \kappa f(\psi, \phi)) \\ &= \beta \left(1 + \frac{\kappa \tilde{f}(\psi, \phi)}{M^2(\kappa + 1)} \right)\end{aligned}\quad (30)$$

where $\tilde{f}(\psi, \phi) = f(\psi, \phi) + M\tilde{v}(\psi, \phi) - M^2$. Note that the larger $\tilde{f}(\psi, \phi)$, the greater $\mathbb{E}[\xi_{\text{aa-is}}^{\text{rf}}]$. However, $\tilde{f}(\psi, \phi) \ll 1$ independently of the value of ϕ as shown in Fig. 3(a) for the case where no preventive adjustment of mean phases is carried out, e.g., $\psi = \mathbf{0}$.

Remark 5: Therefore, channel mean phase shifts do not strictly bias the average harvested energy, which is intuitively expected since transmitted signals are independent to each other. Meanwhile, such result is very different from what happened under the AA-SS scheme for which mean phase shifts always influenced (negatively) on such metric.

Additionally, note that when R_Σ is maximum (perfect correlation), AA-SS could provide up to M times more energy on average than AA-IS, whose average statistics are not affected in any way by R_Σ . The previous statement holds as long as there is no strong LOS component; however, as κ takes greater values, which is typical of WET systems due to the short-range characteristics, $f(\psi, \phi)$ and $\tilde{f}(\psi, \phi)$ become more relevant, which favors the AA-IS scheme.

Let us investigate now the impact on the variance as follows:

$$\begin{aligned}\text{var}[\xi_{\text{aa-is}}^{\text{rf}}] &\approx \frac{\beta^2}{2M^4(\kappa + 1)^2} \left(\frac{(M^2 - R_\Sigma)^2}{(M - 1)^2} \left(2(M - 1) + \frac{4M(M - 1)\kappa \tilde{v}(\psi, \phi)}{M^2 - R_\Sigma} \right) \right. \\ &\quad \left. + R_\Sigma^2 \left(2 + \frac{4\kappa f(\psi, \phi)}{R_\Sigma} \right) \right)\end{aligned}$$

⁶Note that [33, eq. (39)] describes the distribution of the RF incident power under unshifted mean phases and the SA operation considering the whole block time. Therefore, both (28) and [33, eq. (39)] must match when $\Phi = \mathbf{0}$ according to our discussions in Section III-C.

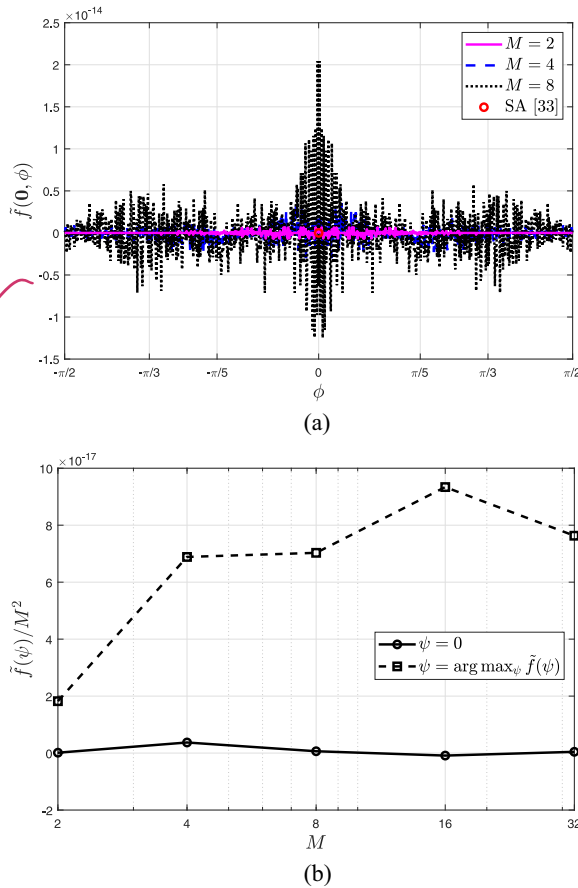


Fig. 3. (a) $\tilde{f}(\mathbf{0}, \phi)$ versus ϕ for $M \in \{2, 4, 8\}$ (top). (b) $\tilde{f}(\psi)$ vs M for $\psi = \mathbf{0}$ and $\psi = \arg \max_{\psi} \tilde{f}(\psi)$ (bottom).

$$\approx \frac{\beta^2}{M^3(M-1)(\kappa+1)^2} \left(M^3(1+2\kappa) + R_{\Sigma}^2 - 2MR_{\Sigma}(1+\kappa) + 2\kappa M(R_{\Sigma}-M)f(\psi, \phi) \right) \quad (31)$$

where last line comes from taking advantage of $f(\psi, \phi) + M\tilde{v}(\psi, \phi) - M^2 \approx 0 \rightarrow \tilde{v}(\psi, \phi) \approx M - f(\psi, \phi)/M$ to write $\text{var}[\xi_{\text{aa-is}}^{\text{rf}}]$ just as a function of $f(\psi, \phi)$. Since $f(\psi, \phi) \geq 0$, it is obvious that just when $M > R_{\Sigma}$, e.g., negative correlation of some antennas, the system performance benefits from having different mean phases.

B. Preventive Adjustment of Mean Phases

Herein, we discuss how to set the vector ψ for optimizing the system performance. Again, ϕ is taken randomly and uniformly from $[0, 2\pi]$ as in Section IV-B.

1) *Average Energy Maximization:* As shown in Fig. 3(a), channel mean phase shifts do not impact significantly on the average incident RF power. Then, it is intuitively expected that none preventive phase shifting would improve such average statistics. To corroborate this, we require computing $\tilde{f}(\psi) = (1/2\pi) \int_0^{2\pi} \tilde{f}(\psi, \phi) d\phi$, for which

$$\begin{aligned} \tilde{f}(\psi) &= \frac{1}{2\pi} \int_0^{2\pi} f(\psi, \phi) d\phi + \frac{M}{2\pi} \int_0^{2\pi} \tilde{v}(\psi, \phi) d\phi - \frac{M^2}{2\pi} \int_0^{2\pi} d\phi \\ &= f(\psi) - M + \sum_{j=1}^{M-1} \frac{4\pi}{j(j+1)} \end{aligned}$$

$$\begin{aligned} &\times \left(\sum_{t=M-j+1}^{M-1} J_0(t\pi) \cos \psi_t \right. \\ &+ \sum_{t=M-j+1}^{M-1} \sum_{l=t+1}^{M-1} J_0((l-t)\pi) \cos(\psi_t - \psi_l) \\ &- j \sum_{t=M-j+1}^{M-1} J_0((t-M+j)\pi) \cos(\psi_{M-j} - \psi_t) \\ &\left. - jJ_0((M-j)\pi) \cos \psi_{M-j} \right) \quad (32) \end{aligned}$$

where $f(\psi)$ is given in (21) and last line comes from integrating $\tilde{v}(\psi, \phi)$ over ϕ by using the integral representation of $J_0(\cdot)$ [37, eq. (10.9.1)]. Due to the extreme nonlinearity of (32), we resort to exhaustive search optimization solvers of MATLAB to find $\arg \max_{\psi} \tilde{f}(\psi)$ and compare its performance with the nonpreventive phase shifting scheme for which $\psi = \mathbf{0}$. Specifically, we show in Fig. 3(b) their associated performance in terms of $\tilde{f}(\psi)$ normalized by M^2 since the average incident RF power depends strictly on such ratio. Results evidence that although the performance gap is large in relative terms, it is not in absolute values. That is, not even the optimum preventive phase shifting allows increasing $\tilde{f}(\psi)/M^2$ significantly, e.g., $\tilde{f}(\psi)/M^2 \approx 0$. PAMP 对 AA-2S 无关? 不解得 J(\psi) 增加, 可能增加

Remark 6: Then, and based on (30), the average incident RF power is approximately β . Therefore, this scheme cannot take advantage of the multiple antennas to improve the average statistics of the incident RF power in any way. 能解 2S 增加

2) *Energy Dispersion Minimization:* As in Section IV-B2 we consider the variance of the incident RF power as the dispersion measure. Then, we have that

$$\begin{aligned} \arg \min_{\psi} \text{var}[\xi_{\text{aa-is}}^{\text{rf}}] &= \begin{cases} \arg \min_{\psi} f(\psi), & \text{if } R_{\Sigma} > M \\ \arg \max_{\psi} f(\psi), & \text{if } R_{\Sigma} < M \end{cases} \\ &= \begin{cases} \psi \approx \mathbf{0}, & \text{if } R_{\Sigma} > M \\ \psi_t = \text{mod}(t, 2)\pi, & \text{if } R_{\Sigma} < M \end{cases} \quad (33) \end{aligned}$$

where last line comes from using directly our previous results in Section IV-B. In addition, note that $\text{var}[\xi_{\text{aa-is}}^{\text{rf}}]$ is not a function of $f(\psi)$ when $R_{\Sigma} = M$ [see (31)], thus a preventive phase shifting is not necessary as it does not make any difference. R>M Variance 不是 f(ψ) 的函数

Remark 7: Since the average incident RF energy is not affected by any phase shifting, we can conclude that (33) provides the optimum preventive phase shifting. This means that phase shifting is not required when $R_{\Sigma} \geq M$, as in most of the practical systems. 大多都是这样 AA-IS 是随机的所以不用相移

On the other hand, observe from (31) that the variance decreases with M , thus, although the AA-IS is not more advantageous than single antenna transmissions in terms of the provided average RF energy, it benefits significantly from the multiple antennas to reduce the energy dispersion. → AA-2S 能减少能量分散

Finally, based on Section III-C, it is expected that the phase shifting given in (33) approaches the optimum for the SA scheme as well, hence we adopt it in such a scenario. 而且

TABLE I
CSI-FREE SCHEMES AND CORRESPONDING
PREVENTIVE PHASE SHIFTING

Schemes	ψ_t
AA - SS _{max E}	$\text{mod}(t, 2)\pi$
AA - SS _{min var}	0
AA - IS	0
SA	0
"scheme" ($\phi = 0$) [33] (unrealistic)	0 ($\phi = 0$)

TABLE II
SIMULATION PARAMETERS

Parameter	Value
g_{\max}	2 mW
(a, b)	(0.56, 3.5)
ξ_0	-2 dBm
ϕ	uniformly random in $[0, 2\pi]$
κ	5
τ	0.3
M	8

VI. NUMERICAL RESULTS

Herein, we present simulation results on the performance of the discussed CSI-free multiple-antenna schemes under the nonlinear EH model given in (6). We evaluate the average harvested energy,⁷ and energy outage probability, which refers to the probability that the RF energy falls below an energy threshold ξ_0 , thus interrupting the devices' operation.⁸ Notice the energy outage probability is highly related to both mean and variance statistics. The EH hardware parameters agree with the EH circuitry experimental data at 2.45 GHz in [43].

We take ϕ uniformly and randomly from $[0, 2\pi]$, while comparing the corresponding results to those with equal mean phases, $\phi = 0$, which are not attainable in practice and are just presented as a benchmark. For clarity, we summarize the schemes under consideration in Table I. Note that in the case of AA-IS and SA, we just consider the preventive phase shifting given in the first line of (33) since we assume positive spatial correlation, e.g., $R_{\Sigma} \geq M$. Specifically, we assume exponential spatial correlation with coefficient τ such that $R_{i,j} = \tau^{|i-j|}$, hence

$$R_{\Sigma} = M + 2 \sum_{i=1}^{M-1} (M-i)\tau^i = \frac{M(1-\tau^2) - 2\tau(1-\tau^M)}{(1-\tau)^2} \quad (34)$$

where last step comes from using a geometric series compact representation. Such a model is physically reasonable since correlation decreases with increasing distance between antennas. Unless stated otherwise, we set the system parameters as shown in Table II. Note that $\kappa = 5$ and $\tau = 0.3$ to account for certain LOS and correlation, while we assume the PB is equipped with a moderate-to-small number of antennas $M = 8$.

⁷Note that the average PTE is just a scaled version of such average harvested energy for a fixed transmit power, and therefore, its corresponding curves follow the same trends. Similarly, the PDF and CDF of the harvested energy can be easily extrapolated to the statistics of the instantaneous PTE.

⁸ ξ_0 must be obviously not smaller than the EH sensitivity.

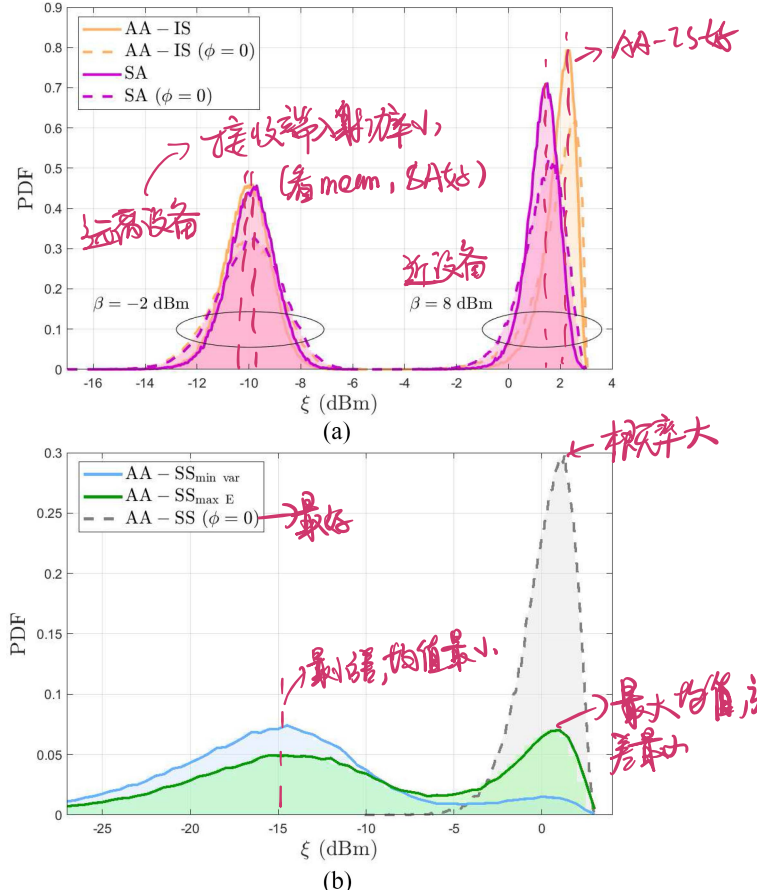
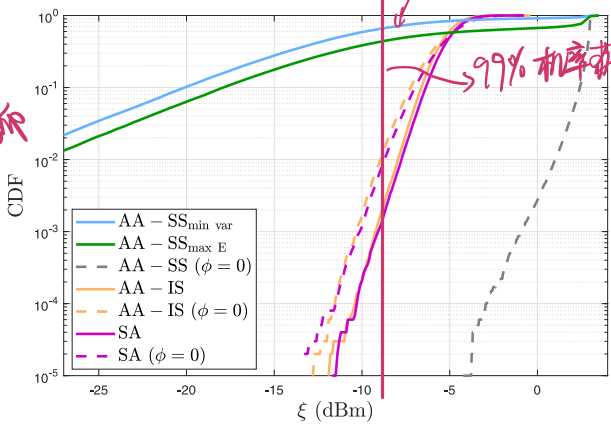


Fig. 4. PDF of the harvested energy: (a) under AA-IS and SA for $\beta \in \{-2, 8\}$ dBm (top) and (b) under AA-SS for $\beta = -2$ dBm (bottom).

A. On the Distribution of the Harvested Energy

In Fig. 4, we illustrate the PDF of the energy harvested under each of the schemes. Specifically, Fig. 4(a) shows the PDF for two different path-loss profiles while considering AA-IS and SA schemes. We observe that under SA, the harvested energy under large path loss presents slightly better statistics than under AA-IS, while AA-IS is superior when operating under better average channel statistics. Therefore, we corroborate our statements in Remark 1: devices far from the PB indeed benefit more from SA than from AA-IS, while those closer to the PB benefit more from the latter. We also show that the statistics improve by considering the channel mean phases, therefore, the performance of these schemes is better in a practical setup than foreseen by [33]. Something different occurs under AA-SS as shown in Fig. 4(b). As we discussed in Section IV, the unshifted mean phase assumption is most optimistic under the operation of AA-SS, and note that the performance gains with respect to what can be attained in practice, e.g., under the AA-SS_{min var} and AA-SS_{max E} discussed in this work, are extremely notorious. Regarding AA-SS_{max E} vs AA-SS_{min var}, we can observe the performance gains in terms of average and variance of the harvested energy, respectively, of one with respect to the other. We must say that although AA-SS_{min var} provides less disperse harvested energy values, they could be extremely small compared to the ones achievable under AA-SS_{max E}. Remark 1

圆点标注

Fig. 5. CDF of the harvested energy for $\beta = 2$ dBm.

Let us analyze now the CDF curves, which are shown in Fig. 5 for $\beta = 2$ dBm.⁹ Note that although with greater variance, AA-SS_{max} E performs superior¹⁰ than AA-SS_{min} var. In fact, this holds in most scenarios, which highlights the need of a π -phase shifting in consecutive antennas when using the AA-SS scheme as foreseen in Remark 3. Meanwhile, the greatest diversity order is attained by AA-IS and SA schemes, which perform similarly. In this case, AA-IS performs slightly superior but this depends greatly on the path loss according to our discussions in the previous paragraph. Note that these two schemes guarantee, for instance, chances above 99% of harvesting more than -8 dBm of power, compared to just 60% and 40% when using AA-SS_{max} E and AA-SS_{min} var, respectively. Once again, the gaps with respect to the performance under unshifted mean phases are evidenced and are shown to be enormous, especially when transmitting the same signal simultaneously by all antennas.

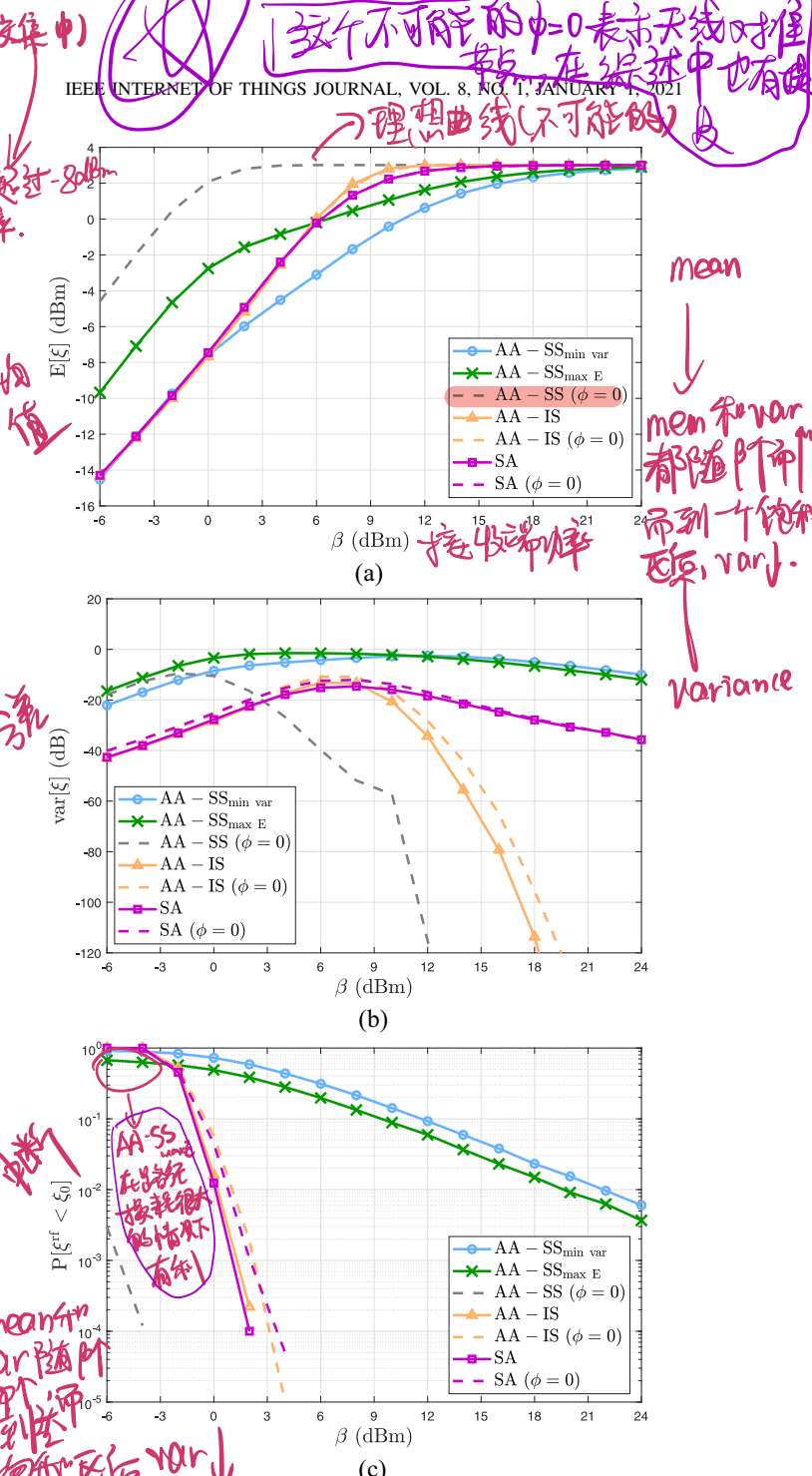
B. On the Impact of the Channel

Fig. 6 shows the average [Fig. 6(a)] and variance [Fig. 6(b)] of the harvested energy, and the energy outage probability [Fig. 6(c)], as a function of the path loss. In general, both the average and variance of the incident RF power increases with β for all schemes. However, the saturation phenomenon captured by (6) makes that the average harvested energy saturates at some point, while obviously the variance would decrease from that point onward. These phenomena are observed in Fig. 6(a) and (b). Note that AA-SS_{max} E achieves considerable gains in terms of average harvested energy compared to AA-SS_{min} var.¹¹ In fact, the performance curve of AA-SS_{max} E lies approximately in the middle between the curves of AA-SS_{min} var and the idealistic AA-SS ($\phi = 0$). Meanwhile, in terms of variance and energy outage probability, they do not

⁹In this and most of the subsequent figures, we adopt $\beta = 2$ dBm to illustrate the performance in the desired operation range, e.g., above/below sensitivity/saturation, since for an incident RF power of 2 dBm (1.6 mW), the harvested power becomes -5.5 dBm (0.28 mW).

¹⁰In this context, a superior performance means that the corresponding CDF curve is below.

¹¹Based on Remark 4 statement, specifically on (24) and (25), and (18), AA-SS_{max} E provides $\sim (\beta\kappa/\kappa + 1)(0.85\sqrt{M} - 0.64)$ more energy units than AA-SS_{min} var on average.

Fig. 6. (a) Average harvested energy (top). (b) Variance of the harvested energy (middle). (c) Energy outage probability (bottom), as a function of β .

中断：AA-IS/SA vs AA-IS.
differ significantly. Regarding AA-IS and SA, we can observe that they even outperform AA-SS_{min} var's performance, while AA-SS_{max} E is strictly superior in the regions of large path loss. Therefore, far devices are the most benefited from AA-SS_{max} E. Meanwhile, since the variance of the incident RF energy [and also harvested energy as observed in Fig. 6(b)] is the lowest under AA-IS and SA, they are capable of providing more stable energy supply, which when operating near (or in) saturation makes the devices to harvest more energy on average when compared to AA-SS_{max} E. That is why the average harvested energy under AA-IS and SA is the greatest among the practical schemes for $\beta > 6$ dBm. Specifically,

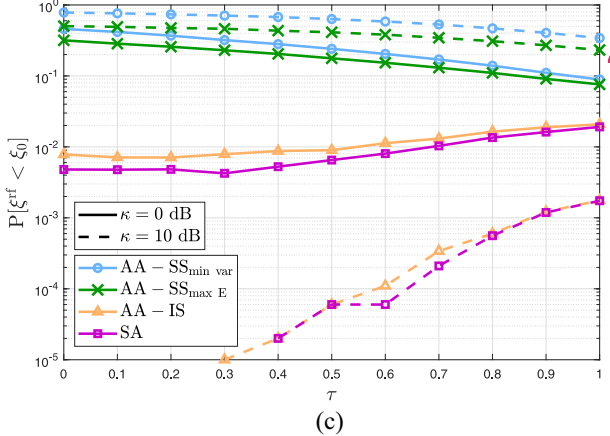
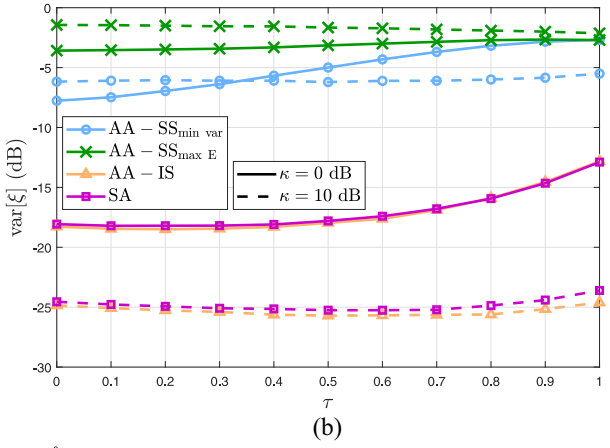
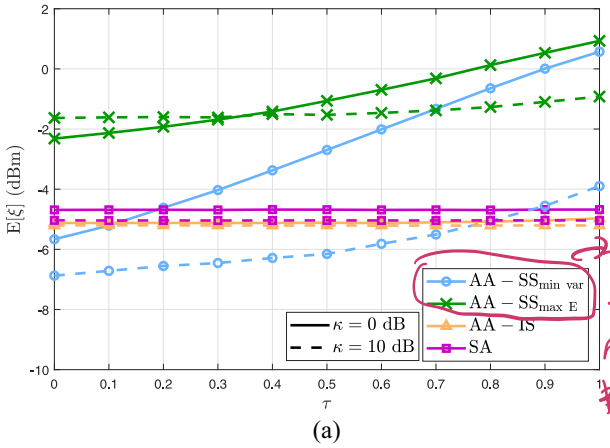


Fig. 7. (a) Average harvested energy (top). (b) Variance of the harvested energy (middle). (c) Energy outage probability (bottom), as a function of τ for $\kappa = \{0, 10\}$ dB and $\beta = 2$ dBm.

AA-IS performs the best in that region while SA is slightly better than AA-IS for $\beta < 4$ dBm. Discussions on this were carried out already in Sections III-C and VI-A.

As we already demonstrated and verified the necessity of considering the mean phase shifts in the analysis, from now on we just focus on showing the performance results under random mean phase shifts, e.g., we dispense of “scheme” ($\phi = 0$) performance curves.

In Fig. 7, we show the statistics [average in Fig. 7(a) and variance in Fig. 7(b)] of the harvested energy, and the energy outage probability [Fig. 7(c)], as a function of the exponential correlation coefficient for two LOS profiles. As evidenced,

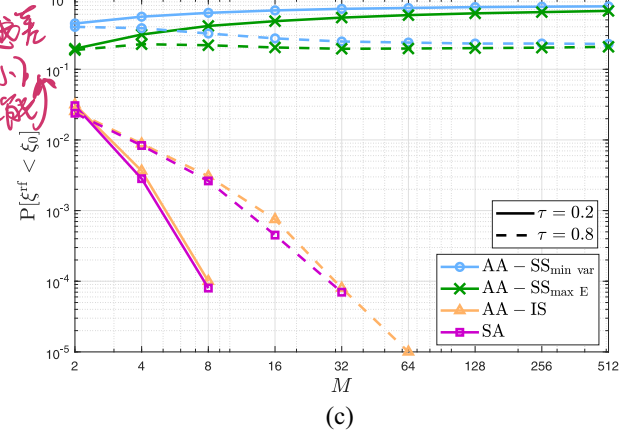
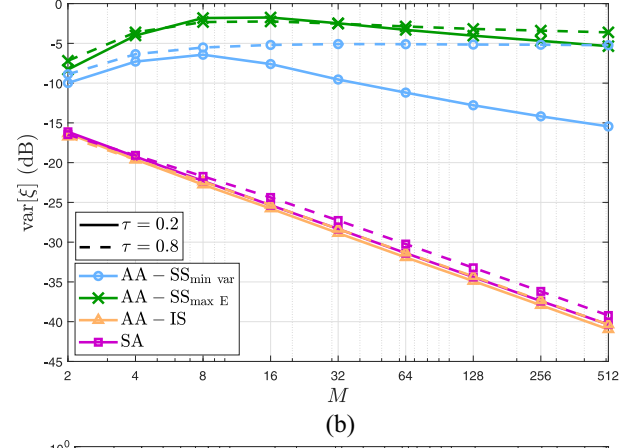
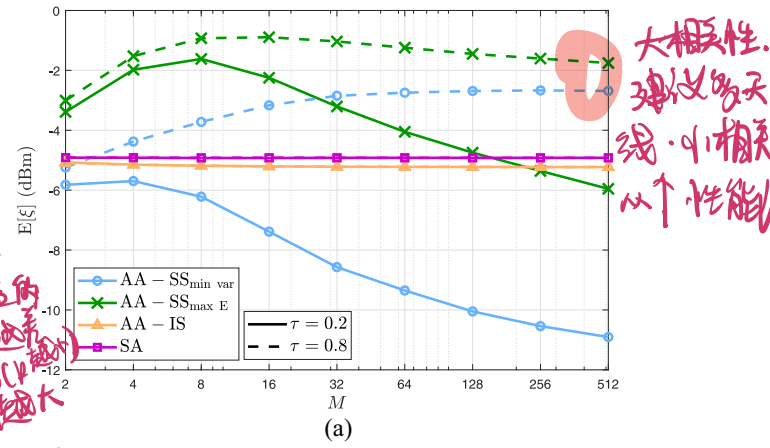


Fig. 8. (a) Average harvested energy (top). (b) Variance of the harvested energy (middle). (c) Energy outage probability (bottom), as a function of M for $\tau = \{0.2, 0.8\}$ and $\beta = 2$ dBm.

a greater correlation is beneficial under the AA-SS schemes, especially under poor LOS where channels are more random. A very counter-intuitive result is that LOS is not always beneficial when transmitting the same signal simultaneously through all antennas. In fact, the energy outage probability under such schemes is lower for $\kappa = 0$ dB than for $\kappa = 10$ dB, which also holds in the case of the average harvested energy when preventive phase shifting is not used, e.g., AA-SS_{min} var, and for $\tau > 0.35$ in the case of AA-SS_{max}E. Meanwhile, since correlation (LOS) is well known to decrease (increase) the diversity, AA-IS and SA schemes are affected by (benefited from) an increasing τ (κ) as shown in Fig. 7(b) and (c). Notice,

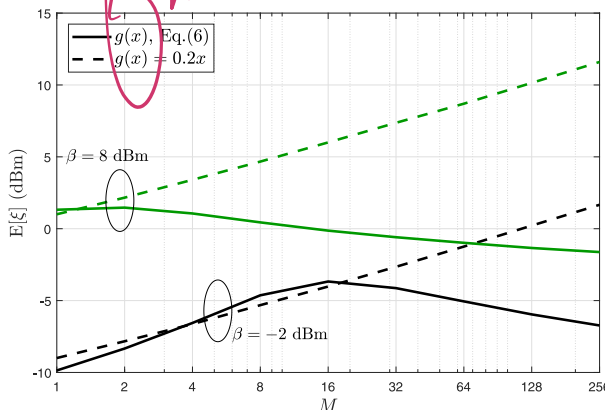


Fig. 9. Average harvested energy as a function of M for $\beta = \{-2, 8\}$ dBm. Nonlinear EH model vs linear EH model with $\eta = 20\%$.

however, that as claimed in Remark 6, the average statistics of the energy harvested under such schemes are not affected in any way by the correlation and only a bit by the LOS factor due to the nonlinearity of the energy harvester. In general, AA-SS_{max E} is the clear winner in terms of maximum average harvested energy, while AA-IS and SA schemes offer better performance in terms of energy outage.

C. On the Impact of the Number of Antennas

Herein, we investigate the impact of the number of transmit antennas on the system performance. Fig. 8 show the average [Fig. 8(a)] and variance [Fig. 8(b)] of the harvested energy, and the energy outage probability [Fig. 8(c)] for $\tau = \{0.2, 0.8\}$. As expected, the average harvested energy under AA-IS and SA remains constant as M increases, while the variance and consequently, the energy outage probability decrease. The latter improves as τ decreases as commented in the previous section. Meanwhile, it is observed that a greater M does not always allows improvements on the system performance when transmitting the same signal simultaneously through all antennas. Interestingly, as the correlation increases a greater number of antennas is advisable, which does not occur for small τ .

Results in Fig. 8 evidence that there is an optimum number of transmit antennas M^* . For instance, in terms of average harvested energy, $M^* = 4$ (8) and $M^* = 256$ (16) for $\tau = 0.2$ and $\tau = 0.8$, respectively, and under the operation of AA-SS_{min var} (AA-SS_{max E}). Such phenomenon is mostly due to the fact that as M increases, the chances of operating close to the minima of $f(\psi, \theta)$ increase for a random θ (see Remark 2), while the maximums cannot be fully exploited due to the nonlinearity of the EH circuitry, specifically due to the saturation phenomenon. To deepen this, we show in Fig. 9 the average harvested energy as a function of M for two different path loss profiles while comparing the performance under the nonlinear EH function to the one attained under the ideal linear EH model with 20% of PTE.¹² Note that the performance grows unbounded under such ideal model, which also happens when analyzing the average incident RF power. However, under the nonlinearities of the energy harvester that is no longer the case.

¹²Instead of the maximum PTE we utilized a more conservative value.

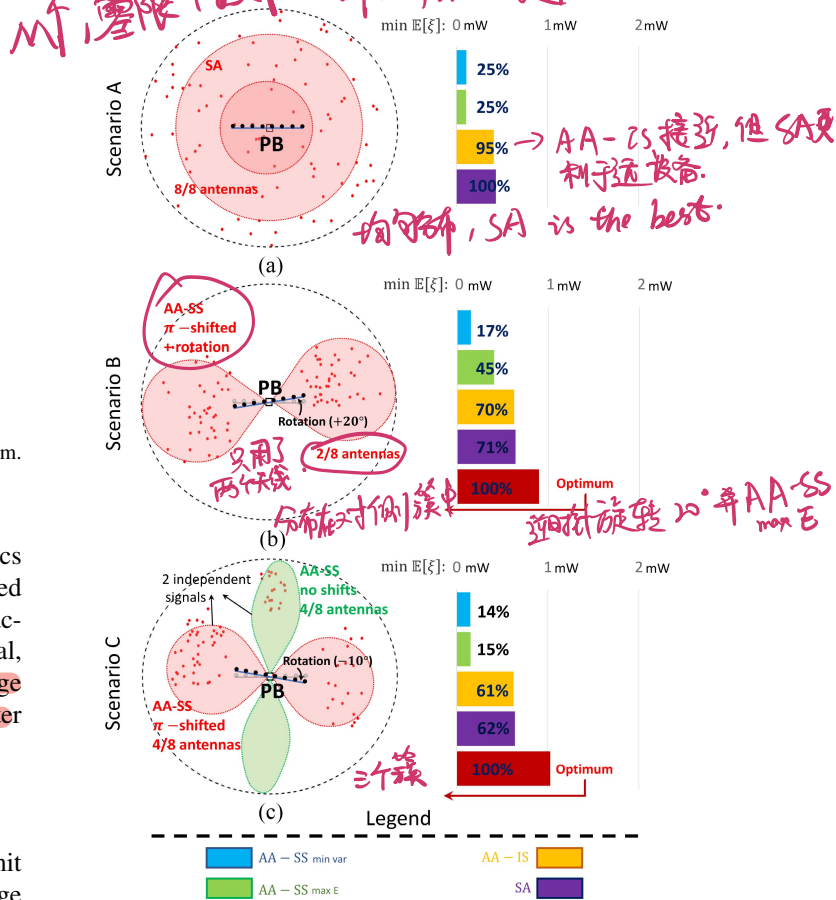


Fig. 10. Devices' minimum harvested energy for three different scenarios: a) devices distributed uniformly in the area, b) devices distributed in two clusters, and c) devices distributed in three clusters. The optimum powering scheme is illustrated together with each scenario. The shown radiation patterns are by no means exhaustive and are included for reference only.

Since for $\beta = -6$ dBm, the device is likely to be operating close to saturation, the optimum number of antennas is small, e.g., $M^* = 1$ or 2, but under greater path loss, such number goes up to $M^* = 16$.

D. Exploiting Positioning Information

Throughout the article, we have assumed that the EH devices are distributed uniformly around the PB, either because their locations are unknown or their deployment distribution is nearly homogeneous. Herein, we show that even when such assumptions do not hold we can still benefit from the analyzed CSI-free powering schemes. As for the performance metric, we adopt the devices' minimum average harvested energy, e.g., worst node's performance, hence, we aim to reveal the max-min fairest scheme for wirelessly powering the three example scenarios depicted in Fig. 10. For all of them, we assume a PB serving a 10-m radius circular area where 80 EH devices¹³ are: 1) scenario A: distributed

¹³Note that WET is usually practical at a scale of a few meters to tens of meters, thus, a 10-m radius area is a valid assumption. Also, the projections toward 6G point to challenging scenarios with up to 10 devices/m² [44], [45], thus the considered 80 deployed EH devices do not constitute a very large number compared to what is expected ten years from now. Obviously, the larger the number of EH devices is, the more beneficial the analyzed CSI-free schemes are when compared to the traditional CSI-based schemes [33].

uniformly in the area; 2) scenario B: distributed in two clusters on opposite sides of the PB; and 3) scenario C: distributed in three clusters, two clusters as in scenario B plus another cluster shifted $\sim 90^\circ$ with respect to the previous. Finally, we model the average RF power available at certain distance d from the PB as β (dBm) = $30 - 27 \log_{10} d(m)$, which may correspond to setups where the PB's total transmit power is 1 W, and channels are subject to log-distance path losses with exponent 2.7.

As evidenced by scenario A, SA constitutes the fairest scheme when the nodes are distributed over the whole area, e.g., without obvious clustering patterns. Note that although AA-IS attains a similar performance, SA is preferable since it favors the farthest devices with EH hardware operating close to the sensitivity region. Meanwhile, AA-SS_{min var} and AA-SS_{max E} are in clear disadvantage because of their performance minima at different angular directions as illustrated in Fig. 1.

Conversely, if the devices are deployed as in scenario B, the optimum strategy requires to rotate the PB's antenna array¹⁴ 20° counter clockwise and then use AA-SS_{max E}.

Note that this is more convenient than for instance rotating the antenna array 70° clockwise and using AA-SS_{min var} since this scheme provides narrower beams and thus powering more dispersed clusters becomes less efficient. Also, just two (consecutive) out of the eight available antennas are utilized such that the side beams are sufficiently wide to efficiently cover all the EH devices. By doing so, the worst-performing device can harvest up to 1.5 dB more energy than under the SA scheme. Similarly, the optimum strategy in scenario C demands a 10° clockwise rotation of the PB's antenna array. Meanwhile, since the devices are now grouped into clusters at $\sim 0^\circ$, $\sim 90^\circ$, and $\sim 180^\circ$, two independent signals can generate the required beams to power them, as illustrated in Fig. 10. Each signal is transmitted with equal power over four (consecutive) out of the eight antennas. The signals are transmitted, respectively, according to the schemes AA-SS_{min var} and AA-SS_{max E} such that all the clusters can be efficiently reached. By doing so, the worst-performing device can harvest up to 2 dB more energy than under the SA scheme.

All WET schemes analyzed in this article aim at powering massive deployments of EH devices without costly CSI acquisition overheads. The results suggest the following.

1) SA and AA-IS are preferable when the devices' deployments are not clustered, e.g., for powering dense deployments of sensors and RFIDs in the warehouse's storage areas. As highlighted in Remark 1 and discussed in previous sections, the specific choice depends on the EH operation region of the critical EH devices, e.g., devices farthest from the PB or those with more stringent energy demands;

2) AA-SS is preferable when devices are clustered in specific spatial directions; e.g., for powering parking lot sensors.

¹⁴This may be possible in static setups, where the task is committed to the technician/user, or in slow-varying environments, where the PB itself is equipped with rotary-motor skills and it is capable of adjusting its orientation.

VII. CONCLUSION

In this article, we analyzed CSI-free schemes that a dedicated multiantenna power station can utilize when powering wirelessly a large set of single-antenna devices. Different from our early work [33], such CSI-free schemes were studied in a more practical setup that takes into account the mean phase shifts between antenna elements. In addition to AA-SS and SAs [33] schemes, we analyzed the AA-IS scheme as well. We demonstrated that those devices far from the PB and more likely to operate near their sensitivity level, benefit more from the SA scheme than from AA-IS. However, those closer to the PB and more likely to operate near saturation, benefit more from AA-IS.

We characterized the distribution of the RF energy at the EH receiver in correlated Rician fading channels under each WET scheme and found out that while AA-IS and SA cannot take advantage of the multiple antennas to improve the average statistics of the incident RF power, the energy dispersion can be significantly reduced. Meanwhile, the gains in terms of average RF energy depend critically on the mean phase shifts between the antenna elements when using AA-SS. In that regard, we show the considerable performance gaps between the idealistic AA-SS studied in [33] and this scheme when considering channels with different mean phases. Even under such performance degradation AA-SS still provides the greatest average RF energy when compared to AA-IS and SA, although its associated energy outage probability is generally the worst. Those tradeoffs make AA-IS and SA schemes suitable for powering devices under HTT/cooperate-like protocols, while AA-SS seems more appropriate for scenarios where the IoT devices are allowed to accumulate energy.

Additionally, we attained the preventive phase shifting that the power station could utilize for maximizing the average energy delivery or minimizing its dispersion for each of the schemes. Specifically, consecutive antennas must be π -phase shifted for optimum average energy performance under AA-SS, while under other optimization criteria and/or different schemes, there is no need of carrying out any preventive phase shifting. Numerical results evidenced that correlation is beneficial under AA-SS, while a very counter-intuitive finding was that a greater LOS and/or the number of antennas was not always beneficial under such WET scheme. Meanwhile, both AA-IS and SA schemes benefit from small correlation, and a large number of antennas and LOS. Finally, we showed that AA-SS (SA and AA-IS) is (are) the fairest when devices are (are not) clustered in specific spatial directions. All these are fundamental results that can be used when designing practical WET systems.

APPENDIX A PROOF OF THEOREM 1

Departing from (8) and using (5), the RF power available as input to the energy harvester obeys

$$\begin{aligned}\xi_{\text{aa-ss}}^{\text{rf}} &= \frac{\beta}{M} |\mathbf{1}^T \mathbf{h}_x + i \mathbf{1}^T \mathbf{h}_y|^2 \\ &= \frac{\beta}{M} \left[(\mathbf{1}^T \mathbf{h}_x)^2 + (\mathbf{1}^T \mathbf{h}_y)^2 \right]\end{aligned}$$

$$\begin{aligned} &\stackrel{(a)}{=} \frac{\beta R_{\Sigma}}{2(\kappa+1)M} (\theta_x^2 + \theta_y^2) \\ &\stackrel{(b)}{\sim} \frac{\beta R_{\Sigma}}{2(\kappa+1)M} \chi^2 \left(2, \frac{2\kappa(v_1(\psi, \phi)^2 + v_2(\psi, \phi)^2)}{R_{\Sigma}} \right) \end{aligned} \quad (35)$$

where $R_{\Sigma} = \mathbf{1}^T \mathbf{R} \mathbf{1}$, while v_1 and v_2 are given in (17). Note that (a) comes from setting $\theta_{x,y}^2 = ([2(\kappa+1)]/[R_{\Sigma}]) (\mathbf{1}^T \mathbf{h}_{x,y})^2$, where $\theta_{x,y} \sim \mathcal{N}(\sqrt{(\kappa/R_{\Sigma})}(v_1 \pm v_2), 1)$ since $\mathbf{1}^T \mathbf{h}_{x,y}$ is still a Gaussian RV, where the mean is equal to the sum of the means of each element of vector $\mathbf{h}_{x,y}$, while the variance equals the sum of the elements of covariance matrix $[1/2(\kappa+1)]\mathbf{R}$ [46]. Therefore, the mean and variances are $\sqrt{[\kappa/2(\kappa+1)]}(v_1 \mp v_2)$ and $[R_{\Sigma}/2(\kappa+1)]$, respectively. Then, (b) comes from using the definition of a noncentral chi-squared RV [36, Cap.2] along with simple algebraic transformations. Finally, after using (16) we attain (15). ■

APPENDIX B PROOF OF THEOREM 2

Based on (10), the RF energy available at S under the AA-IS operation is given by

$$\xi_{\text{aa-is}}^{\text{rf}} = \frac{\beta}{M} (\mathbf{h}_x^T \mathbf{h}_x + \mathbf{h}_y^T \mathbf{h}_y) \quad (36)$$

for which we analyze its distribution as follows. Let us define $\mathbf{z}_{x,y} = \sqrt{2(\kappa+1)}\mathbf{R}^{-1/2}(\mathbf{h}_{x,y} - \sqrt{[\kappa/2(\kappa+1)]}\boldsymbol{\omega}_{x,y})$ which is distributed as $\mathcal{N}(\mathbf{0}, \mathbf{I})$, then

$$\begin{aligned} \mathbf{h}_{x,y} &= \frac{1}{\sqrt{2(\kappa+1)}} \mathbf{R}^{1/2} \mathbf{z}_{x,y} + \sqrt{\frac{\kappa}{2(\kappa+1)}} \boldsymbol{\omega}_{x,y} \quad (37) \\ \mathbf{h}_{x,y}^T \mathbf{h}_{x,y} &= \frac{1}{2(\kappa+1)} \left(\mathbf{R}^{1/2} \mathbf{z}_{x,y} + \sqrt{\kappa} \boldsymbol{\omega}_{x,y} \right)^T \left(\mathbf{R}^{1/2} \mathbf{z}_{x,y} + \sqrt{\kappa} \boldsymbol{\omega}_{x,y} \right) \\ &= \frac{1}{2(\kappa+1)} \left(\mathbf{z}_{x,y} + \mathbf{R}^{-1/2} \sqrt{\kappa} \boldsymbol{\omega}_{x,y} \right)^T \\ &\quad \times \mathbf{R} \left(\mathbf{z}_{x,y} + \mathbf{R}^{-1/2} \sqrt{\kappa} \boldsymbol{\omega}_{x,y} \right) \end{aligned} \quad (38)$$

where last step comes from simple algebraic transformations. Note that $\mathbf{R} = \mathbf{Q} \Lambda \mathbf{Q}^T$ is the spectral decomposition of \mathbf{R} [47, Ch. 21], where Λ is a diagonal matrix containing the eigenvalues of \mathbf{R} , and \mathbf{Q} is a matrix whose column vectors are the orthogonalized eigenvectors of \mathbf{R} . In order to find the eigenvalues, $\{\lambda_j\}$, of \mathbf{R} , we require solving $\det(\mathbf{R} - \lambda \mathbf{I}) = 0$ for λ , which is analytical intractable for a general matrix \mathbf{R} . However, there is analytical tractability for the special case of uniform spatial correlation. Note that for the special case of uniformly spatial correlated fading such that the antenna elements are correlated between each other with coefficient ρ ($R_{i,j} = \rho \forall i \neq j$), we have that

$$R_{\Sigma} = M(1 + (M-1)\rho). \quad (39)$$

Also, in order to guarantee that \mathbf{R} is positive semidefinite and consequently a viable covariance matrix, ρ is lower bounded by $-(1/M-1)$ [48], thus $-(1/M-1) \leq \rho \leq 1$ and $0 \leq R_{\Sigma} \leq M^2$. Then, under such correlation model we have that [33, eq. (32)]

$$\Lambda = \text{diag}(1-\rho, \dots, 1-\rho, 1+(M-1)\rho) \quad (40)$$

thus matrix \mathbf{R} is characterized by two different eigenvalues: $1 - \rho$, which is independent of the number of antennas but has multiplicity $M-1$, and $1 + (M-1)\rho$, whose multiplicity is 1 but increases linearly with M . Then, matrix \mathbf{Q}^T can be written as shown in (41), at the bottom of the next page. Such representation can be verified for any M by using specialized software for matrix processing such as MATLAB or Wolfram.

Now, by substituting $\mathbf{R} = \mathbf{Q} \Lambda \mathbf{Q}^T$ into (38) while setting $\zeta_{x,y} = 2(\kappa+1)\mathbf{h}_{x,y}^T \mathbf{h}_{x,y}$ yields

$$\begin{aligned} \zeta_{x,y} &= \left(\mathbf{z}_{x,y} + \sqrt{\kappa} (\mathbf{Q} \Lambda \mathbf{Q}^T)^{-\frac{1}{2}} \boldsymbol{\omega}_{x,y} \right)^T \mathbf{Q} \Lambda \mathbf{Q}^T \\ &\quad \times \left(\mathbf{z}_{x,y} + \sqrt{\kappa} (\mathbf{Q} \Lambda \mathbf{Q}^T)^{-\frac{1}{2}} \boldsymbol{\omega}_{x,y} \right) \\ &\stackrel{(a)}{=} \left(\mathbf{Q}^T \mathbf{z}_{x,y} + \sqrt{\kappa} \Lambda^{-\frac{1}{2}} \mathbf{Q}^T \boldsymbol{\omega}_{x,y} \right)^T \Lambda \\ &\quad \times \left(\mathbf{Q}^T \mathbf{z}_{x,y} + \sqrt{\kappa} \Lambda^{-\frac{1}{2}} \mathbf{Q}^T \boldsymbol{\omega}_{x,y} \right) \\ &\stackrel{(b)}{=} (\mathbf{P}_{x,y} + \sqrt{\kappa} \mathbf{u}_{x,y})^T \Lambda (\mathbf{P}_{x,y} + \sqrt{\kappa} \mathbf{u}_{x,y}) \\ &\stackrel{(c)}{=} \sum_{j=1}^M \lambda_j (c_j + \sqrt{\kappa} u_{x,y,j})^2 \end{aligned} \quad (42)$$

where (a) comes after some algebraic transformations, (b) follows from taking $\mathbf{P}_{x,y} = \mathbf{Q}^T \mathbf{z}_{x,y} \sim \mathcal{N}(\mathbf{0}, \mathbf{I})$, and

$$\begin{aligned} \mathbf{u}_{x,y} &= \Lambda^{-\frac{1}{2}} \mathbf{Q}^T \boldsymbol{\omega}_{x,y} \\ &= \Lambda^{-\frac{1}{2}} \begin{bmatrix} \frac{1}{\sqrt{2}} (\omega_M - \omega_1) \\ \frac{1}{\sqrt{2 \times 3}} (2\omega_{M-1} - \omega_1 - \omega_M) \\ \frac{1}{\sqrt{3 \times 4}} (3\omega_{M-2} - \omega_1 - \sum_{j=M-1}^M \omega_j) \\ \frac{1}{\sqrt{4 \times 5}} (4\omega_{M-3} - \omega_1 - \sum_{j=M-2}^M \omega_j) \\ \vdots \\ \frac{1}{\sqrt{(M-2)(M-1)}} ((M-2)\omega_3 - \omega_1 - \sum_{j=4}^M \omega_j) \\ \frac{1}{\sqrt{(M-1)M}} ((M-1)\omega_2 - \omega_1 - \sum_{j=3}^M \omega_j) \\ \frac{1}{\sqrt{M}} \sum_{j=1}^M \omega_j \end{bmatrix} \end{aligned} \quad (43)$$

$$u_{x,y,j} = \begin{cases} \frac{j\omega_{M-j+1} - \omega_1 - \sum_{t=M-j+2}^M \omega_t}{\sqrt{j(j+1)\lambda_j}}, & \text{for } j \leq M-1 \\ \frac{1}{\sqrt{M\lambda_M}} \sum_{t=1}^M \omega_t, & \text{for } j = M \end{cases} \quad (44)$$

which come from using (40) and (41); while (c) follows after taking $c_j \sim \mathcal{N}(0, 1)$.

By incorporating these results into (36), we obtain the distribution of $\xi_{\text{aa-is}}^{\text{rf}}$ as follows:

$$\begin{aligned} \xi_{\text{aa-is}}^{\text{rf}} &\sim \frac{\beta}{2M(\kappa+1)} (\zeta_x + \zeta_y) \\ &\sim \frac{\beta}{2M(\kappa+1)} \sum_{j=1}^M \lambda_j \left((c_j + \sqrt{\kappa} u_{x,j})^2 + (\tilde{c}_j + \sqrt{\kappa} u_{y,j})^2 \right) \\ &\sim \frac{\beta}{2M(\kappa+1)} \left((1-\rho)\chi^2 \left(2(M-1), \frac{2\kappa\tilde{v}(\psi, \phi)}{1-\rho} \right) \right. \\ &\quad \left. + (1+(M-1)\rho)\chi^2 \left(2, \frac{\kappa f(\psi, \phi)}{M(1+(M-1)\rho)} \right) \right) \end{aligned} \quad (45)$$

since $\tilde{c}_j \sim \mathcal{N}(0, 1)$

$$\begin{aligned} & u_{xM}^2 + u_{yM}^2 \\ &= \frac{1}{M\lambda_M} \left(\left(\sum_{t=1}^M \omega_{xt} \right)^2 + \left(\sum_{t=1}^M \omega_{yt} \right)^2 \right) \\ &= \frac{(v_1(\psi, \phi) - v_2(\psi, \phi))^2 + (v_1(\psi, \phi) + v_2(\psi, \phi))^2}{M(1 + (M-1)\rho)} \\ &= \frac{2f(\psi, \phi)}{M(1 + (M-1)\rho)} \end{aligned} \quad (46)$$

while $\tilde{v} = (1/2) \sum_{j=1}^{M-1} \lambda_j (u_{xj}^2 + u_{yj}^2)$, which appears expanded as a function of ψ and Φ , shown in (47) at the top of the next page, and it is obtained by (a) using (44), (b) expanding the quadratic binomials, and (c) performing some algebraic simplifications by taking advantage of $\sin^2 a + \cos^2 a = 1$. Then, we attain (29) by regrouping terms and performing further algebraic simplifications by taking advantage of $\cos a \cos b + \sin a \sin b = \cos(a-b)$.

Note that (45) holds under the assumption of uniform spatial correlation; however, given that for the AA scheme, we were able of writing the distribution merely as a function of parameter R_Σ , which is not linked to any specific kind of correlation, we can expect that the behavior under the AA-IS scheme depends, at least approximately, on R_Σ rather than the specific entries of matrix \mathbf{R} . In fact, such hypothesis has been shown to be accurate under the scenario of LOS components with equal mean phases studied in [33]. To explore this, we substitute $\rho = [(R_\Sigma - M)/M(M-1)]$ coming from (39), into (45), such that we attain (28). ■

APPENDIX C VALIDATION

To evaluate the accuracy of (28), we utilize the Bhattacharyya distance metric [49], which measures the similarity of two probability distributions \mathbf{p}_1 and \mathbf{p}_2 , and it is given by

$$d_B(\mathbf{p}_1, \mathbf{p}_2) = -\ln(c_B(\mathbf{p}_1, \mathbf{p}_2)) \quad (48)$$

where c_B is the Bhattacharyya coefficient [49]. In the case of our interest, both probability distributions characterize ξ_{aa-is}^{rf} ; however, for \mathbf{p}_1 we assume a uniform spatial correlation matrix \mathbf{R} , thus we may use (28) which is exact in such scenario; while for \mathbf{p}_2 we assume a randomly generated correlation matrix \mathbf{R}^* such that $R_\Sigma = R_\Sigma^*$, thus we

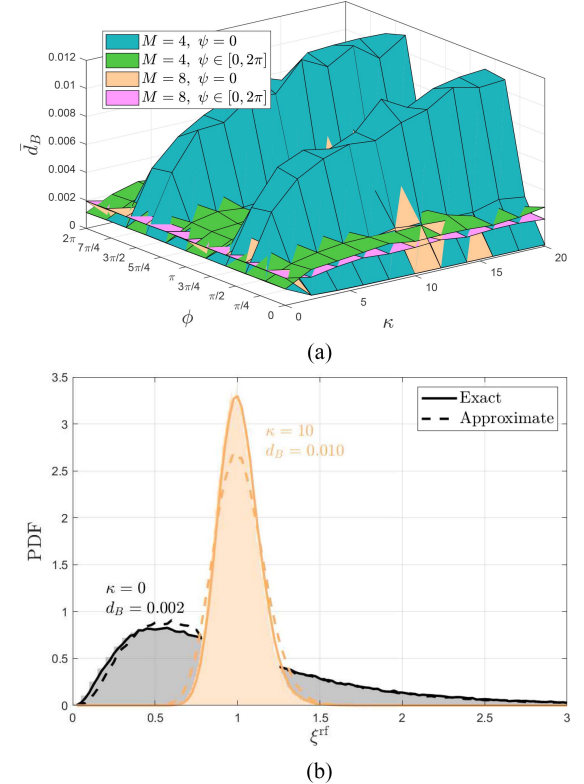


Fig. 11. (a) Average Bhattacharyya distance between $\hat{\mathbf{p}}_1$ and $\hat{\mathbf{p}}_2$ as a function of κ and ϕ for $M \in \{4, 8\}$, $\psi = \mathbf{0}$ (no preventive phase shifting) and ψ taken uniformly random from $[0, 2\pi]^{M-1}$ (top). (b) Monte Carlo-based comparison between the exact \mathbf{p}_2 and proposed approximate \mathbf{p}_1 distributions of the incident RF power under the AA – IS scheme. We set $M = 4$, $\phi = 3\pi/4$ and $\psi = \mathbf{0}$. The comparison is carried out for two different cases: 1) $\kappa = 0$, $d_B = 0.002$ and 2) $\kappa = 10$, $d_B = 0.010$ (bottom).

evaluate the distribution directly from (36). We utilize the histogram formulation for estimating \mathbf{p}_1 and \mathbf{p}_2 . Specifically, we estimate $\hat{\mathbf{p}}_1 = \{\hat{p}_{1,i}\}_{i=1,\dots,m}$ (with $\sum_{i=1}^m \hat{p}_{1,i} = 1$) and $\hat{\mathbf{p}}_2 = \{\hat{p}_{2,i}\}_{i=1,\dots,m}$ (with $\sum_{i=1}^m \hat{p}_{2,i} = 1$), where m is the number of histogram bins. Then, the Bhattacharyya coefficient is calculated as [49]

$$c_B(\hat{\mathbf{p}}_1, \hat{\mathbf{p}}_2) = \sum_{i=1}^m \sqrt{\hat{p}_{1,i} \hat{p}_{2,i}}. \quad (49)$$

By substituting (49) into (48), we calculate the similarity between distributions. Note that according to (28), we have that $d_B(\mathbf{p}_1, \mathbf{p}_2) \in [0, \infty)$, where 0 corresponds to the case when $\mathbf{p}_1 = \mathbf{p}_2$.

$$\mathbf{Q}^T = \begin{bmatrix} -\frac{1}{\sqrt{1 \times 2}} & 0 & 0 & \dots & 0 & 0 & 0 & \frac{1}{\sqrt{1 \times 2}} \\ -\frac{1}{\sqrt{2 \times 3}} & 0 & 0 & \dots & 0 & 0 & \frac{2}{\sqrt{2 \times 3}} & -\frac{1}{\sqrt{2 \times 3}} \\ -\frac{1}{\sqrt{3 \times 4}} & 0 & 0 & \dots & 0 & \frac{3}{\sqrt{3 \times 4}} & -\frac{1}{\sqrt{3 \times 4}} & -\frac{1}{\sqrt{3 \times 4}} \\ -\frac{1}{\sqrt{4 \times 5}} & 0 & 0 & \dots & \frac{4}{\sqrt{4 \times 5}} & -\frac{1}{\sqrt{4 \times 5}} & -\frac{1}{\sqrt{4 \times 4}} & -\frac{1}{\sqrt{4 \times 5}} \\ \vdots & \vdots & \vdots & \ddots & \vdots & \vdots & \vdots & \vdots \\ -\frac{1}{\sqrt{(M-2)(M-1)}} & 0 & \frac{M-2}{\sqrt{(M-2)(M-1)}} & \dots & -\frac{1}{\sqrt{(M-2)(M-1)}} & -\frac{1}{\sqrt{(M-2)(M-1)}} & -\frac{1}{\sqrt{(M-2)(M-1)}} & -\frac{1}{\sqrt{(M-2)(M-1)}} \\ -\frac{1}{\sqrt{(M-1)M}} & \frac{M-1}{\sqrt{(M-1)M}} & -\frac{1}{\sqrt{(M-1)M}} & \dots & -\frac{1}{\sqrt{(M-1)M}} & -\frac{1}{\sqrt{(M-1)M}} & -\frac{1}{\sqrt{(M-1)M}} & -\frac{1}{\sqrt{(M-1)M}} \\ \frac{1}{\sqrt{M}} & \frac{1}{\sqrt{M}} & \frac{1}{\sqrt{M}} & \dots & \frac{1}{\sqrt{M}} & \frac{1}{\sqrt{M}} & \frac{1}{\sqrt{M}} & \frac{1}{\sqrt{M}} \end{bmatrix} \quad (41)$$

$$\begin{aligned}
\tilde{v}(\psi, \phi) &\stackrel{(a)}{=} \sum_{j=1}^{M-1} \frac{1}{2j(j+1)} \left(\left(j\omega_{xM-j+1} - \omega_{x1} - \sum_{t=M-j+2}^M \omega_{xt} \right)^2 + \left(j\omega_{yM-j+1} - \omega_{y1} - \sum_{t=M-j+2}^M \omega_{yt} \right)^2 \right) \\
&\stackrel{(b)}{=} \sum_{j=1}^{M-1} \frac{1}{2j(j+1)} \left(j^2 (\omega_{xM-j+1}^2 + \omega_{yM-j+1}^2) + 2 + \left(\sum_{t=M-j+2}^M \omega_{xt} \right)^2 + \left(\sum_{t=M-j+2}^M \omega_{yt} \right)^2 - 2j(\omega_{xM-j+1} + \omega_{yM-j+1}) \right. \\
&\quad \left. - 2j \left(\omega_{xM-j+1} \sum_{t=M-j+2}^M \omega_{xt} + \omega_{yM-j+1} \sum_{t=M-j+2}^M \omega_{yt} \right) + 2 \sum_{t=M-j+2}^M (\omega_{xt} + \omega_{yt}) \right) \\
&\stackrel{(c)}{=} \sum_{j=1}^{M-1} \frac{1}{j(j+1)} \left(\left(\sum_{t=M-j+1}^{M-1} \cos(\psi_t + \Phi_t) \right)^2 + \left(\sum_{t=M-j+1}^{M-1} \sin(\psi_t + \Phi_t) \right)^2 + j^2 + 1 - 2j \cos(\psi_{M-j} + \Phi_{M-j}) \right. \\
&\quad \left. - 2j \left(\cos(\psi_{M-j} + \Phi_{M-j}) \sum_{t=M-j+1}^{M-1} \cos(\psi_t + \Phi_t) + \sin(\psi_{M-j} + \Phi_{M-j}) \sum_{t=M-j+1}^{M-1} \sin(\psi_t + \Phi_t) \right) \right. \\
&\quad \left. + 2 \sum_{t=M-j+1}^{M-1} \cos(\psi_t + \Phi_t) \right)
\end{aligned} \tag{47}$$

Fig. 11(a) shows the average Bhattacharyya distance, \bar{d}_B , as a function of κ and ϕ for $M \in \{4, 8\}$, $\psi = \mathbf{0}$ (no preventive phase shifting) and ψ taken uniformly random from $[0, 2\pi]^{M-1}$ to account for different possible preventive phase shiftings. We generated 1000 random correlation matrices and averaged over the Bhattacharyya distance for the distributions corresponding to each of them. We utilized 2×10^5 distribution samples and set $m = 240$, while the histogram edges were uniformly chosen between 0 and 6, which is an appropriate range since, without loss of generality, we used $\beta = 1$. As observed in the figure, the largest difference between both distributions is when $\psi = \mathbf{0}$, M is small, e.g., $M = 4$, and $\phi \approx \pi/4 \pm \pi/2$. In such scenario, \bar{d}_B increases with κ ; however, according to further extensive simulations although d_B values become close to 0.012 they never surpass such limit. Meanwhile, for other parameter configurations \bar{d}_B becomes significantly smaller.

We select $\bar{d}_B = 0.010$ and $\bar{d}_B = 0.002$ to illustrate the cases of, respectively, large and small differences between the considered distributions in Fig. 11(b). Note that the approximate distributions indeed approach the exact ones, even with greater accuracy for smaller d_B as expected. Finally, since $\bar{d}_B = 0.010$ is a very pessimistic assumption as it is only reachable for few values of ϕ , results in Fig. 11(b) validate the accuracy of (28) in general scenarios.

REFERENCES

- [1] M. Shirvanimoghaddam, M. Dohler, and S. J. Johnson, "Massive non-orthogonal multiple access for cellular IoT: Potentials and limitations," *IEEE Commun. Mag.*, vol. 55, no. 9, pp. 55–61, Sep. 2017.
- [2] X. Wang, C. Lu, F. Wang, W. Xu, and S. Li, "Research status of wireless power transmission technology," in *Communications, Signal Processing, and Systems*, Q. Liang, W. Wang, X. Liu, Z. Na, M. Jia, and B. Zhang, Eds. Singapore: Springer, 2020, pp. 731–738.
- [3] S. H. Chae, C. Jeong, and S. H. Lim, "Simultaneous wireless information and power transfer for Internet of Things sensor networks," *IEEE Internet Things J.*, vol. 5, no. 4, pp. 2829–2843, Aug. 2018.
- [4] Z. Hou, H. Chen, Y. Li, and B. Vucetic, "Incentive mechanism design for wireless energy harvesting-based Internet of Things," *IEEE Internet Things J.*, vol. 5, no. 4, pp. 2620–2632, Aug. 2018.
- [5] W. Saad, M. Bennis, and M. Chen, "A vision of 6G wireless systems: Applications, trends, technologies, and open research problems," *IEEE Netw.*, vol. 34, no. 3, pp. 134–142, May/Jun. 2020.
- [6] O. L. A. López, H. Alves, R. D. Souza, S. Montej-Sánchez, E. M. G. Fernández, and M. Latva-Aho. (2019). *Massive Wireless Energy Transfer: Enabling Sustainable IoT Towards 6G Era*. [Online]. Available: <https://arxiv.org/pdf/1912.05322.pdf>
- [7] L.-G. Tran, H.-K. Cha, and W.-T. Park, "RF power harvesting: A review on designing methodologies and applications," *Micro Nano Syst. Lett.*, vol. 5, no. 1, p. 14, Feb. 2017.
- [8] H. Jayakumar, K. Lee, W. S. Lee, A. Raha, Y. Kim, and V. Raghunathan, "Powering the Internet of Things," in *Proc. IEEE/ACM Int. Symp. Low Power Electron. Design*, 2014, pp. 375–380.
- [9] Y. Zhang *et al.*, "A batteryless 19 μ W MICS/ISM-band energy harvesting body sensor node SoC for ExG applications," *IEEE J. Solid-State Circuits*, vol. 48, no. 1, pp. 199–213, Jan. 2013.
- [10] T. Zhang, M. Law, P. Mak, M. Vai, and R. P. Martins, "Nano-watt class energy-efficient capacitive sensor interface with on-chip temperature drift compensation," *IEEE Sensors J.*, vol. 18, no. 7, pp. 2870–2882, Apr. 2018.
- [11] Y. Alazzawi, O. Chatterjee, and S. Chakrabarty, "A compact and energy-efficient ultrasound receiver using PTAT reference circuit," *Microelectron. J.*, vol. 94, Dec. 2019, Art. no. 104656.
- [12] F. Moreno-Cruz, V. T. Lopez, F. J. Romero, C. Hambeck, D. P. Morales, and A. Rivadeneira, "Use of low-cost printed sensors with RF energy harvesting for IoT," in *Proc. Smart Syst. Integration*, Apr. 2019, pp. 1–4.
- [13] B. Clerckx, R. Zhang, R. Schober, D. W. K. Ng, D. I. Kim, and H. V. Poor, "Fundamentals of wireless information and power transfer: From RF energy harvester models to signal and system designs," *IEEE J. Sel. Areas Commun.*, vol. 37, no. 1, pp. 4–33, Jan. 2019.
- [14] S. Bi, Y. Zeng, and R. Zhang, "Wireless powered communication networks: An overview," *IEEE Wireless Commun.*, vol. 23, no. 2, pp. 10–18, Apr. 2016.
- [15] H. Ju and R. Zhang, "Throughput maximization in wireless powered communication networks," *IEEE Trans. Wireless Commun.*, vol. 13, no. 1, pp. 418–428, Jan. 2014.
- [16] O. L. A. López, H. Alves, R. D. Souza, and E. M. G. Fernández, "Ultrareliable short-packet communications with wireless energy transfer," *IEEE Signal Process. Lett.*, vol. 24, no. 4, pp. 387–391, Apr. 2017.

- [17] O. L. A. López, H. Alves, R. D. Souza, S. Montejo-Sánchez, and E. M. G. Fernández, "Rate control for wireless-powered communication network with reliability and delay constraints," *IEEE Trans. Wireless Commun.*, vol. 18, no. 12, pp. 5791–5805, Dec. 2019.
- [18] H. Chen, Y. Li, J. L. Rebelatto, B. F. Uchôa-Filho, and B. Vucetic, "Harvest-then-cooperate: Wireless-powered cooperative communications," *IEEE Trans. Signal Process.*, vol. 63, no. 7, pp. 1700–1711, Apr. 2015.
- [19] O. L. A. López, E. M. G. Fernández, R. D. Souza, and H. Alves, "Ultra-reliable cooperative short-packet communications with wireless energy transfer," *IEEE Sensors J.*, vol. 18, no. 5, pp. 2161–2177, Mar. 2018.
- [20] O. L. A. López, R. D. Souza, H. Alves, and E. M. G. Fernández, "Ultra reliable short message relaying with wireless power transfer," in *Proc. IEEE Int. Conf. Commun.*, May 2017, pp. 1–6.
- [21] O. L. A. López, E. M. G. Fernández, R. D. Souza, and H. Alves, "Wireless powered communications with finite battery and finite blocklength," *IEEE Trans. Commun.*, vol. 66, no. 4, pp. 1803–1816, Apr. 2018.
- [22] B. T. Bacinoglu, O. Kaya, and E. Uysal-Biyikoglu, "Energy efficient transmission scheduling for channel-adaptive wireless energy transfer," in *Proc. IEEE Wireless Commun. Netw. Conf.*, Apr. 2018, pp. 1–6.
- [23] Z. Yang, W. Xu, Y. Pan, C. Pan, and M. Chen, "Energy efficient resource allocation in machine-to-machine communications with multiple access and energy harvesting for IoT," *IEEE Internet Things J.*, vol. 5, no. 1, pp. 229–245, Feb. 2018.
- [24] H. Li, K. Ota, and M. Dong, "Energy cooperation in battery-free wireless communications with radio frequency energy harvesting," *ACM Trans. Embedded Comput. Syst.*, vol. 17, no. 2, pp. 44, pp. 1–44:17, Feb. 2018.
- [25] K. Huang and V. K. N. Lau, "Enabling wireless power transfer in cellular networks: Architecture, modeling and deployment," *IEEE Trans. Wireless Commun.*, vol. 13, no. 2, pp. 902–912, Feb. 2014.
- [26] W. Huang, H. Chen, Y. Li, and B. Vucetic, "On the performance of multi-antenna wireless-powered communications with energy beamforming," *IEEE Trans. Veh. Technol.*, vol. 65, no. 3, pp. 1801–1808, Mar. 2016.
- [27] J. Park, Y. Jeon, and S. Han, "Energy beamforming for wireless power transfer in MISO heterogeneous network with power beacon," *IEEE Commun. Lett.*, vol. 21, no. 5, pp. 1163–1166, May 2017.
- [28] Y. Zeng and R. Zhang, "Optimized training design for wireless energy transfer," *IEEE Trans. Commun.*, vol. 63, no. 2, pp. 536–550, Feb. 2015.
- [29] Y. Zeng and R. Zhang, "Optimized training for net energy maximization in multi-antenna wireless energy transfer over frequency-selective channel," *IEEE Trans. Commun.*, vol. 63, no. 6, pp. 2360–2373, Jun. 2015.
- [30] S. Bi and R. Zhang, "Placement optimization of energy and information access points in wireless powered communication networks," *IEEE Trans. Wireless Commun.*, vol. 15, no. 3, pp. 2351–2364, Mar. 2016.
- [31] Y. Chen, N. Zhao, and M. Alouini, "Wireless energy harvesting using signals from multiple fading channels," *IEEE Trans. Commun.*, vol. 65, no. 11, pp. 5027–5039, Nov. 2017.
- [32] B. Clerckx and J. Kim, "On the beneficial roles of fading and transmit diversity in wireless power transfer with nonlinear energy harvesting," *IEEE Trans. Wireless Commun.*, vol. 17, no. 11, pp. 7731–7743, Nov. 2018.
- [33] O. L. A. López, H. Alves, R. D. Souza, and S. Montejo-Sánchez, "Statistical analysis of multiple antenna strategies for wireless energy transfer," *IEEE Trans. Commun.*, vol. 67, no. 10, pp. 7245–7262, Oct. 2019.
- [34] C. He, Z. J. Wang, and V. C. M. Leung, "Unitary query for the $M \times L \times N$ MIMO backscatter RFID channel," *IEEE Trans. Wireless Commun.*, vol. 14, no. 5, pp. 2613–2625, May 2015.
- [35] C. He, Z. J. Wang, C. Miao, and V. C. M. Leung, "Block-level unitary query: Enabling orthogonal-like space-time code with query diversity for MIMO backscatter RFID," *IEEE Trans. Wireless Commun.*, vol. 15, no. 3, pp. 1937–1949, Mar. 2016.
- [36] J. Proakis, *Digital Communications*. Boston, MA, USA: McGraw-Hill, 2001.
- [37] I. Thompson, *NIST Handbook of Mathematical Functions*, 1st ed. Cambridge, U.K.: Cambridge Univ. Press, May 2011.
- [38] J. R. Hampton, *Introduction to MIMO Communications*. Cambridge, U.K.: Cambridge Univ. Press, 2013.
- [39] P. J. Schreier and L. L. Scharf, *Statistical Signal Processing of Complex-Valued Data: The Theory of Improper and Noncircular Signals*. Cambridge, U.K.: Cambridge Univ. Press, 2010.
- [40] M. A. Khalighi, J. . Brossier, G. Jourdain, and K. Raoof, "On capacity of Rician MIMO channels," in *Proc. IEEE Int. Symp. Pers. Indoor Mobile Radio Commun.*, vol. 1, Oct. 2001, pp. 150–154.
- [41] B. Clerckx and E. Bayguzina, "Waveform design for wireless power transfer," *IEEE Trans. Signal Process.*, vol. 64, no. 23, pp. 6313–6328, Dec. 2016.
- [42] E. Boshkovska, D. W. K. Ng, N. Zlatanov, and R. Schober, "Practical non-linear energy harvesting model and resource allocation for SWIPT systems," *IEEE Commun. Lett.*, vol. 19, no. 12, pp. 2082–2085, Dec. 2015.
- [43] D. Khan *et al.*, "A CMOS RF energy harvester with 47% peak efficiency using internal threshold voltage compensation," *IEEE Microw. Wireless Compon. Lett.*, vol. 29, no. 6, pp. 415–417, Jun. 2019.
- [44] N. H. Mahmood, H. Alves, O. A. López, M. Shehab, D. P. M. Osorio, and M. Latva-Aho. (2019). *Six Key Enablers for Machine Type Communication in 6G*. [Online]. Available: <https://arxiv.org/abs/1903.05406>
- [45] N. H. Mahmood et al. (2020). *White Paper on Critical and Massive Machine Type Communication Towards 6G*. [Online]. Available: <https://arxiv.org/abs/2004.14146>
- [46] A. Novosyolov, *The Sum of Dependent Normal Variables May Be Not Normal*, Inst. Comput. Model., Siberian Branch Russian Acad. Sci., Krasnoyarsk, Russia, 2006.
- [47] D. Harville, *Matrix Algebra From a Statistician's Perspective*. New York, NY, USA: Springer-Verlag, 2008.
- [48] X. Chen, "Antenna correlation and its impact on multi-antenna system," *Progr. Electromagn. Res.*, vol. 62, pp. 241–253, Mar. 2015.
- [49] T. Kailath, "The divergence and Bhattacharyya distance measures in signal selection," *IEEE Trans. Commun. Technol.*, vol. 15, no. 1, pp. 52–60, Feb. 1967.

Onel L. A. López (Member, IEEE) received the B.Sc. degree (First Class Hons.) in electrical engineering from the Central University of Las Villas, Santa Clara, Cuba, in 2013, the M.Sc. degree from the Federal University of Paraná, Curitiba, Brazil, in 2017, and the D.Sc. degree (with Distinction) from the University of Oulu, Oulu, Finland, in 2020.

He is an Active Postdoctoral Researcher of machine-type wireless communications, sustainable networks, and cellular wireless systems with the Centre for Wireless Communications, University of Oulu.

Dr. López is a co-recipient of the IEEE European Conference on Networks and Communications Best Student Paper Award in 2019 and a collaborator to the Research Award given by the Cuban Academy of Sciences in 2016.

Samuel Montejo-Sánchez (Member, IEEE) was born in Camaguey, Cuba, in 1979. He received the B.Sc., M.Sc., and D.Sc. degrees in telecommunications from the Central University of Las Villas (UCLV), Santa Clara, Cuba, in 2003, 2007, and 2013, respectively.

From September 2003 to May 2017, he was an Associate Professor with the Department of Telecommunications, UCLV. From February 2011 to July 2011, he was a visiting Ph.D. student with the Federal University of Technology, Apucarana, Brazil. In 2017, he held a postdoctoral position with the University of Chile, Santiago, Chile. Since 2018, he has been with the Programa Institucional de Fomento a la I+D+i, Universidad Tecnológica Metropolitana, Santiago. His research interests are in the areas of wireless communications, cognitive radio, network coding, energy efficiency, vehicular *ad hoc* networks, physical layer security, machine-type communication, and Internet of Things.

Dr. Montejo-Sánchez was a co-recipient of the Research Award from the Cuban Academy of Sciences in 2016. He is a member of FONDECYT Regular 1201893 (IoT goes to Space: Wireless Networking Protocols and Architectures for IoT Networks served by LEO satellite constellations), STIC AnSud 19-STIC-08 (Visible Light Mine Communications—VLmC), FONDEQUIP EQM180180 (Clúster Supermicro para Cómputo Científico), and UTEM L318-04 (Clúster de Computación Acelerada por GPU) projects.

Richard D. Souza (Senior Member, IEEE) received the D.Sc. degree in electrical engineering from the Federal University of Santa Catarina (UFSC), Florianópolis, Brazil, in 2003.

From 2004 to 2016, he was with the Federal University of Technology—Paraná, Apucarana, Brazil. Since 2017, he has been with UFSC, where he is an Associate Professor. His research interests are in the areas of wireless communications and signal processing.

Dr. Souza is a co-recipient of the IEEE/IFIP Wireless Days Conference Best Paper Award in 2014, the supervisor of the awarded Best Ph.D. Thesis in electrical engineering in Brazil, in 2014, and the co-recipient of the Research Award from the Cuban Academy of Sciences in 2016. He has served as an Associate Editor for IEEE COMMUNICATIONS LETTERS, the IEEE TRANSACTIONS ON VEHICULAR TECHNOLOGY, and the IEEE INTERNET OF THINGS JOURNAL.

Constantinos B. Papadias (Fellow, IEEE) received the Diploma degree in electrical engineering from the National Technical University of Athens, Athens, Greece, in 1991, and the Doctoral degree (Highest Hons.) in signal processing from the Ecole Nationale Supérieure des Télécommunications, Paris, France, in 1995.

He was the Dean/Scientific Director with Athens Information Technology, Athens, where he was also the Head of the Broadband Wireless and Sensor Networks Research Group. He is the Founding Executive Director of the Research, Technology and Innovation Network (RTIN), American College of Greece, Athens, where he has also been a Professor of information technology since February 2020 and also founded and heads RTIN's Smart Wireless Future Technologies Lab. He currently holds Adjunct Professorships with the ACG's Alba Graduate School of Business, Aalborg University, Aalborg, Denmark, and the University of Cyprus, Nicosia, Cyprus. He was a Researcher with the Institut Eurécom, Biot, France, from 1992 to 1995, Stanford University, Stanford, CA, USA, from 1995 to 1997, and Bell Labs, Murray Hill, NJ, USA (as a Member of Technical Staff from 1997 to 2001 and as a Technical Manager from 2001 to 2006). He was also an Adjunct Professor with Columbia University, New York, NY, USA, from 2004 to 2005, and Carnegie Mellon University, Pittsburgh, PA, USA, from 2006 to 2011. He has published over 200 papers and four books and has received over 9400 citations for his work, with an H-index of 44. He has also made standards contributions and holds 12 patents.

Dr. Papadias was a member of the Steering Board of the Wireless World Research Forum from 2002 to 2006, the industrial liaison of the IEEE's Signal Processing for Communications Technical Committee from 2003 to 2008, and the National Representative of Greece to the European Research Council's IDEAS Program from 2007 to 2008. He has served as a member of the IEEE Communications Society's Fellow Evaluation and Awards Committees, as well as an associate editor for various journals. He has contributed to the organization of several conferences, including as the General Chair of IEEE CTW 2016 and IEEE SPAWC 2018 workshops. He has acted as a Technical Coordinator in several EU projects, such as the CROWN in the area of cognitive radio; the HIATUS in the area of interference alignment; the HARP in the area of remote radio heads; and the ADEL in the area of licensed shared access. He is currently the Research Coordinator of the European Training Network Project PAINLESS on the topic of energy autonomous infrastructure-less wireless networks and the Technical Coordinator of the EU CHIST-ERA Project FIREMAN on the topic of predictive maintenance via machine-type wireless communication systems. He was a Distinguished Lecturer of the IEEE Communications Society from 2012 to 2013. He was appointed a Fellow of the European Alliance of Innovation in 2019.

Hirley Alves (Member, IEEE) received the B.Sc. and M.Sc. degrees in electrical engineering from the Federal University of Technology—Paraná (UTFPR), Apucarana, Brazil, in 2010 and 2011, respectively, and the dual D.Sc. degree from the University of Oulu, Oulu, Finland, and UTFPR in 2015.

In 2017, he was an Adjunct Professor of machine-type wireless communications with the Centre for Wireless Communications (CWC), University of Oulu, where he joined CWC as an Assistant Professor in 2019 and is currently the Head of the Machine-Type Wireless Communications Group. He is actively working on massive connectivity and ultrareliable low-latency communications for future wireless networks, 5G and 6G, full-duplex communications, and physical-layer security. He leads the URLLC activities for the 6G Flagship Program.

Dr. Alves is a co-recipient of the IEEE International Symposium on Wireless Communications and Systems Best Student Paper Award in 2017 and the Research Award from the Cuban Academy of Sciences in 2016. He has been the organizer, chair, TPC, and tutorial lecturer for several renowned international conferences. He was the General Chair of ISWCS'2019 and the Co-Chair of the first 6G Summit, Levi 2019.